International Journal of Nanomedicine

Dovepress
Taylor & Francis Group

Open Access Full Text Article

ORIGINAL RESEARCH

Carrier-Free, Hyaluronic Acid-Modified Self-Assembled Doxorubicin, and Chlorin e6 Nanoparticles Enhance Combined Chemo- and Photodynamic Therapy in vivo

BeiBei Lin, Peizhen Lin, Xiaobi Zhang, Yingyi Liao, Yinfei Yu, Xuegu Xu, Xiaoling Wang

State Key Laboratory of Ophthalmology, Optometry and Visual Science, National Clinical Research Center for Ocular Diseases, Eye Hospital, Wenzhou Medical University, Wenzhou, Zhejiang, People's Republic of China

Correspondence: Xuegu Xu; Xiaoling Wang, Tel +86-0577-8806-8864, Email xuexuegu@eye.ac.cn; ysgwxl@eye.ac.cn

Background: Developing carrier-free nanomedicines via self-assembly of two antitumor drug molecules is a potential strategy for enhancing the combination treatment of tumors. Similarly, conventional chemotherapy combined with photodynamic therapy may synergistically improve the antitumor effect while minimizing the adverse reactions associated with antitumor treatment. Hyaluronic acid (HA) can bind to overexpressed HA receptors on the tumor cell surface, increasing cell internalization and resulting in good tumor-targeting properties.

Methods: Herein, we propose an easy and environmentally friendly approach for fabricating a novel formulation of carrier-free pure nanodrugs through self-assembly of the antitumor drug doxorubicin (DOX) and the photosensitizer chlorin e6 (Ce6), followed by sequential modification with HA to achieve simultaneous and targeted photodynamic therapy and chemotherapy.

Results: The fabricated HA-DOX-Ce6 nanoparticles (NPs) exhibited enhanced drug loading and stability while possessing the properties of near-infrared fluorescence imaging, self-targeting drug delivery, and combined photodynamic therapy and chemotherapy.

Conclusions: HA-DOX-Ce6 NPs, along with laser irradiation, effectively suppressed tumor development both in vitro and in vivo with minimal side effects. Overall, this biomaterial-based, carrier-free drug delivery system, in combination with cotargeted therapies, has shown potential for considerable improvements in treatment outcomes and patient prognosis.

Keywords: carrier-free, self-assembly, hyaluronic acid, cancer targeting, chemotherapy, photodynamic therapy

Introduction

Tumors are fatal disorders and major mortality-inducing factors worldwide.[1] Chemotherapy, one of the main methods for treating tumors, has been extensively used for treating different tumors. However, despite extensive drug discoveries, most anticancer drugs exhibit low solubility, poor stability, high clearance in the body, and a lack of targeted ability, leading to severe side effects.[2–4] Hence, mechanisms to optimize the physicochemical properties of chemotherapeutic agents to improve their efficacy and lower their toxicity need further investigation.

In recent years, various developments in nanotechnology have shown that nanoparticles (NPs) exhibit great potential as drug carriers. Various studies have been conducted to establish diverse nanoscale drug delivery systems (DDSs), including liposomes, solid lipid NPs, dendrimers, micelles, polymeric NPs, and inorganic nanomaterials, which have been suggested for potential applications.[3,5–7] The drug is adsorbed or covalently attached to the surface of the nanocarrier or encapsulated into it, which may improve the physicochemical properties of the drug, protect the drug from rapid clearance, increase the site-specific drug concentration, and reduce its adverse effects, making the nanocarrier-associated drug a superior candidate for more effective and safe treatment of cancers.[8–10] Despite the notable advantages of DDSs, certain problems, such as their low drug-loading capacity, limit their clinical application. The carrier weight is

Received: 21 September 2024
Accepted: 23 December 2024
Published: 31 December 2024

a major component of nanoformulations, which are larger than the drug weight, resulting in a general drug-loading rate of <10%.[11–13] Additionally, potential carrier-induced systemic toxicity and corresponding biodegradation issues are important. Drug carriers are usually inert and inactive, as they are primarily used as delivery vehicles; nonetheless, they can increase the systemic toxicity of pharmaceutical preparations, and their degradation at a later period may also cause problems, further increasing the burden on patients. Hence, many nanoformulations have not been approved by the Food and Drug Administration.[14] Furthermore, some DDSs require complex multistep preparation processes or organic solvents, which usually show obvious toxicity.[15] Therefore, problems such as adverse reactions caused by organic solvents, complex preparations, challenging formulation scale-up processes, and low cost-effectiveness are still major concerns.

To avoid such DDS-associated problems, the development of carrier-free pure nanodrugs (PNDs), which exclusively contain molecules with pharmacologic activity, has garnered considerable attention. Typically, an environmentally friendly and simple supramolecular self-assembly technique can be utilized for fabricating PND nanoformulations.[16–18] Using this emerging strategy, different chemotherapeutic drugs, such as paclitaxel, doxorubicin (DOX), and curcumin, have been self-assembled into PNDs to enhance anticancer therapies.[19] Notably, PDN shows great promise for more effective and safer cancer treatment.

Most tumors are not efficiently suppressed or grow slowly under a single treatment method, such as chemotherapy.[20] For better therapeutic effects in clinical settings, combination treatment strategies have been widely adopted, and different anticancer drugs are used to coordinate tumor treatment.[21,22] The appropriate combination of compounds can synergistically target tissues to promote therapeutic effects.[23,24] In recent years, the combination of conventional chemotherapy and photodynamic therapy (PDT) has shown great potential for synergistically improving anticancer efficacy and reducing the therapeutic dose of chemotherapeutic drugs to minimize side effects.[25–27] Additionally, combining PDT with chemotherapy may address other chemotherapy-associated problems, such as multidrug resistance-mediated failure.[28,29] Clinical application also shows that PDT combined with chemotherapy has notable advantages in improving the treatment effect for patients in the late stages.[25]

Therefore, herein, we propose an easy and environmentally friendly approach for fabricating a novel PND formulation via self-assembly of the antitumor agent DOX and the photosensitizer chlorin e6 (Ce6) for simultaneous PDT and chemotherapy. Additionally, the self-assembled DOX and Ce6 were polymerized into NPs (DOX-Ce6 NPs) through electrostatic, hydrophobic, and π-π stacking interactions without the involvement of organic solvents. For tumor targeting, the hyaluronic acid (HA) moiety, which targets the cluster of differentiation (CD)44 receptor, was coupled onto the surface of the DOX-Ce6 NPs. Figure 1 shows the preparation scheme for HA-coupled DOX-Ce6 NPs (HA-DOX-Ce6 NPs). The HA-DOX-Ce6 NPs designed in this study may be used to treat cancer in vivo more safely and effectively.

Materials and Methods

Materials

Ce6, DOX hydrochloride, HA (molecular weight = 6.3 kDa), 3-(4,5-dimethylthiazol-2-yl)-2,5-diphenyltetrazolium bromide (MTT), 1,3-diphenylisobenzofuran (DPBF), and 2',7'-dichlorodihydrofluorescein diacetate (DCFH-DA) were procured from Sigma-Aldrich (Steinheim, Germany). N-hydroxysuccinimide and 1-ethyl-3-(3-dimethylaminopropyl)-carbodiimide hydrochloride (EDC·HCl) were obtained from Aladdin Reagent (Shanghai, China). 4,6-Diamidino-2-phenylindole dihydrochloride (DAPI), LysoTracker Red, and Annexin V-fluorescein isothiocyanate (FITC)/propidium iodide (PI) were obtained from Beyotime Biotechnology (Haimen, China). High-glucose Dulbecco's modified Eagle's medium (DMEM) and fetal bovine serum (FBS) were obtained from Gibco (USA).

Six-week-old male BALB/c-nude mice were provided by Zhejiang Provincial Animal Center (Zhejiang, China). The animal experiments were performed in accordance with the Wenzhou Medical University guidelines for the welfare and ethics of experimental animals, and all the animal experimental procedures were performed with the approval of the Animal Experimental Ethics Committee of Wenzhou Medical University (approval number: YSG23102601). Human colorectal cancer HCT-116 cells were obtained from Wuhan Pricella Biotechnology Co., Ltd. (Wuhan, China).

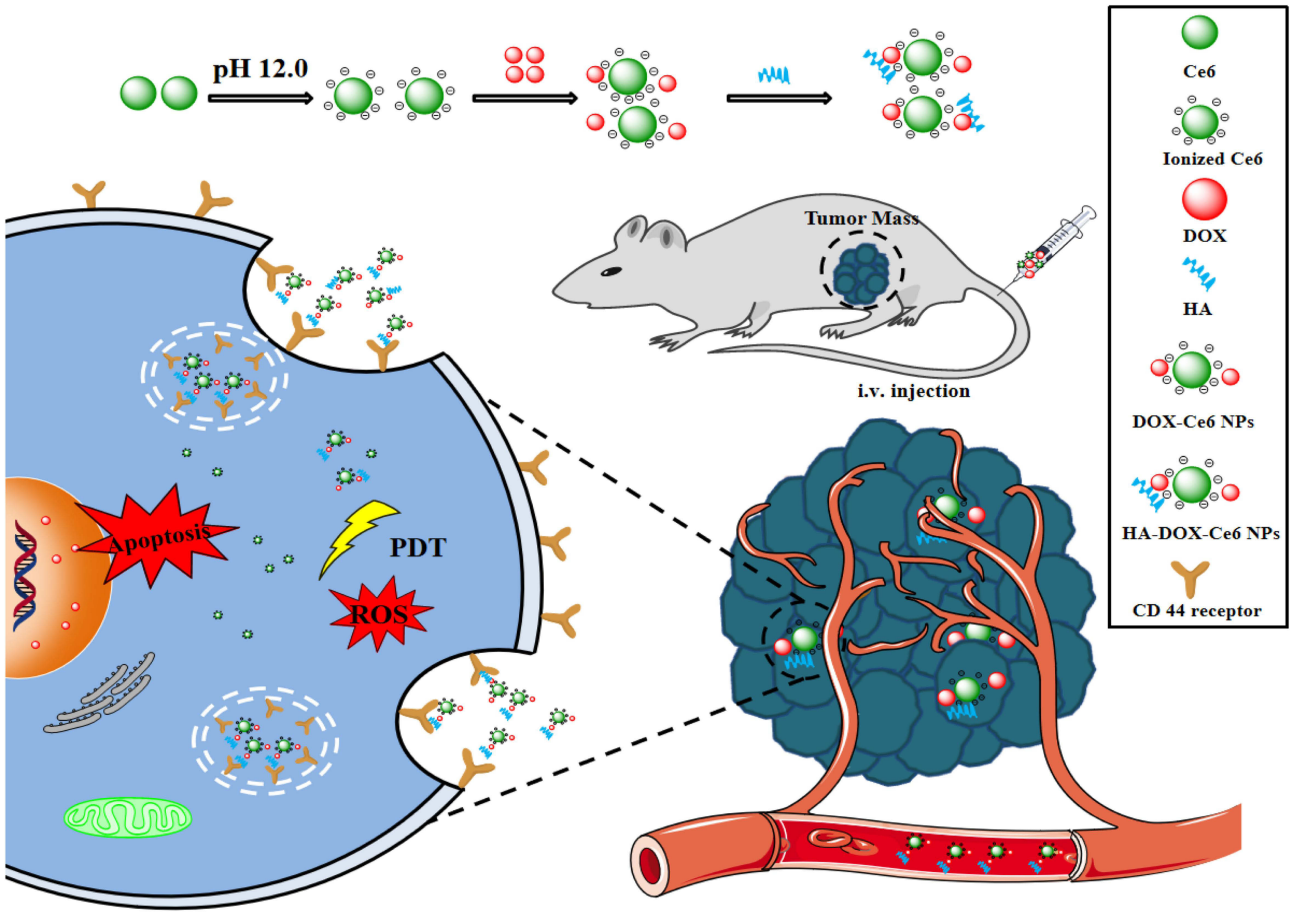

Figure 1 Carrier-free and self-assembled nanoparticles containing DOX and Ce6 decorated with HA with improved antitumor efficacy by combining chemotherapy and PDT in vivo.

Preparation and Characterization of HA-DOX-Ce6 NPs

Figure 2 illustrates the HA-DOX-Ce6 NP synthesis procedure. First, DOX-Ce6 NPs were prepared using a simple self-assembly approach through electrostatic, hydrophobic, and π-π stacking interactions.[30] Briefly, 0.4 mg of Ce6 was dissolved in 400 μL of NaOH (pH = 12) for alkalization for 10 min. Subsequently, a DOX solution (20 μL, 10 mg/mL) was added dropwise to the resulting solution, and deionized (DI) water was added to make up a 1 mL volume immediately. After 24 h of stirring at 37 °C, the DOX-Ce6 NPs were harvested, centrifuged at 12,000 rpm, and lyophilized before collection.

HA-DOX-Ce6 NPs were subsequently fabricated via electrostatic interactions between HA and DOX.[31] DOX-Ce6 NPs (2 mL; 1 mg/mL) were added to 1 mL of 5 mg/mL HA solution, followed by 4 h of stirring at room temperature. Excess HA was removed through 24-h dialysis (molecular weight cutoff [MWCO] = 10–12 kDa) against DI water. Finally, HA-DOX-Ce6 NPs were obtained after lyophilization.

The effects of the DOX/Ce6 ratio (1:2, 1:1, 2:1, or 3:1) or the initial concentration of the DOX solution (10, 15, or 20 mg/mL) on the drug loading and encapsulation efficiency, particle size, and polydispersity index (PDI) were subsequently determined.

HA-DOX-Ce6 NPs were dispersed in phosphate-buffered saline (PBS), and a microplate reader (Multiskan GO, Thermo Fisher Scientific, MA, USA) was used to record the ultraviolet (UV)–visible (Vis) spectra at room temperature. Additionally, a Nicolet 6700 Fourier transform infrared (FT-IR) spectrometer was used to acquire the FT-IR spectra via the potassium bromide approach.

https://doi.org/10.2147/IJN.S490485

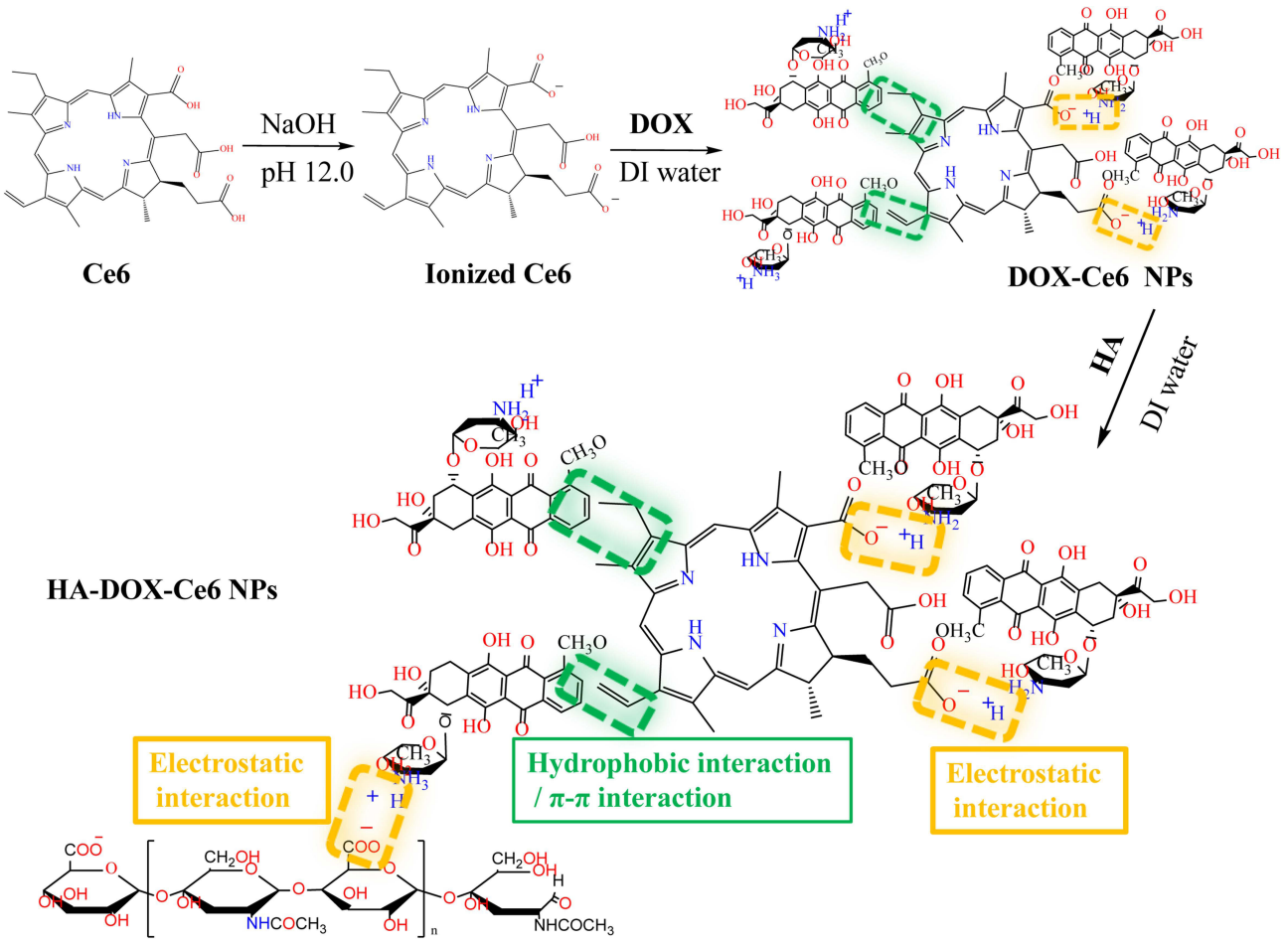

Figure 2 Synthesis of HA-DOX-Ce6 NPs.

HA-DOX-Ce6 NPs were subjected to redispersion in PBS (pH 7.4), and their morphologies were observed through transmission electron microscopy (TEM; TEM-EM400). The HA-DOX-Ce6 NP morphology was also observed through scanning electron microscopy (SEM; Phenom Nano, The Netherlands). A Zetasizer Nano ZS90 (Malvern, UK) was used to determine the particle size and zeta potential.

Additionally, we characterized the encapsulation efficiency (EE) and drug-loading efficiency (LE) of HA-DOX-Ce6 NPs. Lyophilized NPs were added to 0.2% sodium dodecyl sulfate and sonicated for 5 min. Subsequently, the Ce6 and DOX contents were determined using a UV-Vis spectrophotometer at 400 and 495 nm, respectively. EE and LE were determined as follows:

$$\mathrm{EE}(\%)=\frac{\text{Encapsulated drug weight in NPs}}{\text{Total drug weight}}\times 100 \tag{1}$$

$$\mathrm{LE}(\%)=\frac{\text{Encapsulated drug weight in NPs}}{\text{NPs Weight}}\times 100 \tag{2}$$

The stability of the HA-DOX-Ce6 NPs was evaluated. HA-DOX-Ce6 NPs were dispersed in PBS and stored at 4 °C for 60 d. The size, zeta potential, *TEM and SEM* were measured immediately. To evaluate the stability against dilutions after being injected, the NPs were diluted with PBS containing 10% serum 10-fold, and the sizes and zeta potentials were evaluated after dilution.

Drug Release Profiles of the HA-DOX-Ce6 NPs

HA-DOX-Ce6 NPs were suspended in PBS (pH 7.4) before being placed into a dialysis bag (MWCO = 3500 Da), which was then immersed in 20 mL of PBS. The samples were subsequently placed into a shaker at 90 rpm at 37 °C. The medium (1.0 mL) was removed at preset time points and replaced with the same amount of freshly prepared medium to maintain conditions. Afterward, the harvested medium was examined using a fluorescence spectrophotometer. The detection parameters were as follows: for DOX, EX = 495 nm and EM = 559 nm; for Ce6, EX = 400 nm and EM = 666 nm. A Ce6 solution dissolved in dimethyl sulfoxide (DMSO) or DOX dissolved in DI water was used as the control.

Reactive Oxygen Species (ROS) Detection

HA-DOX-Ce6 NP-induced in vitro ROS production was detected using DPBF as an indicator.[32] Briefly, HA-DOX-Ce6 NPs containing 20 μM DPBF were irradiated with light at 50 mW/cm^2 (670 nm) for predetermined time intervals. Finally, a fluorescence spectrophotometer was used to record the absorption spectra; the excitation and emission spectra were fixed at 403 nm and 460 nm, respectively.

Cellular Absorption of HA-DOX-Ce6 NPs

Human colorectal cancer cells, namely, HCT-116 cells, were cultivated with high-glucose DMEM containing 10% FBS and 100 IU/mL penicillin/streptomycin and inoculated with 5% CO_2 at 37 °C. To evaluate the cellular uptake of the NPs, HCT-116 cells (5×10^4/well) were inoculated into 24-well plates overnight attachment. Freshly prepared media (500 μL) containing DOX, Ce6, DOX-Ce6 NPs, HA-DOX-Ce6 NPs, and HA-DOX-Ce6 NPs with free HA (molecular weight = 6.3 kDa, 5 mg/mL), with equivalent DOX and Ce6 concentrations of 2 μg/mL and 0.96 μg/mL, respectively, were subsequently added to replace the original medium. After a 4-h incubation, the cells were rinsed three times with PBS, followed by fixation with 4% (w/w) formaldehyde. Finally, DAPI was used for cell staining, and confocal laser scanning microscopy (CLSM; Zeiss LSM880, Germany) was performed for observation.

For quantitative analysis, the cells were washed with PBS, followed by 15 min of lysis with Triton X-100, and the HA-DOX-Ce6 NP levels in the cells were subsequently determined through fluorescence spectrophotometry.

Distribution of HA-DOX-Ce6 NPs in Cells

TEM and CLSM were performed to observe the intracellular distribution of the HA-DOX-Ce6 NPs. Briefly, 1×10^6 HCT-116 cells were subjected to a 4-h incubation with HA-DOX-Ce6 NPs, followed by washing with PBS three times. After trypsinization, the cells were centrifuged and fixed with 2.5% glutaraldehyde at 4 °C before collection. Next, the cells were treated with 3% glutaraldehyde and 1% osmium tetroxide, followed by serial dehydration with acetone. The samples were later embedded with Araldite resin, and glass knives were used to cut ultrathin sections. These sections were observed using TEM after lead nitrate staining.

For CLSM analysis, after a 4-h incubation at 37 °C, HCT-116 cells were rinsed before 1 h of staining with LysoTracker. The cells were then fixed with 4% (w/w) formaldehyde, followed by DAPI nuclear staining and subsequent observation with CLSM.

ROS Production in Cells Under Irradiation

The DCFH-DA probe was used to stain HCT-116 cells to detect ROS levels. Briefly, 5×10^4 cells were inoculated with DOX, Ce6, DOX-Ce6 NPs, or HA-DOX-Ce6 NPs at a Ce6 equivalent concentration. After 4 h of incubation, the cells were rinsed with PBS, followed by 5 min of laser irradiation (50 mW/cm^2) at 670 nm. Finally, after washing with PBS three times, the cells were stained with DCFH-DA (15 μM, PBS). Hoechst (10 μg/mL, PBS) was added for nuclear staining before CLSM analysis.

Cytotoxicity of HA-DOX-Ce6 NPs in vitro

The cytotoxicity of HA-DOX-Ce6 NPs was evaluated in HCT-116 cells using an MTT assay. Briefly, we inoculated HCT-116 cells (1×10^4/well) into a 96-well plate overnight. Then, freshly prepared medium without FBS containing different

concentrations of free DOX solution, free Ce6 solution, DOX-Ce6 NPs, and HA-DOX-Ce6 NPs was added to replace the original medium for 4 h. After incubation for 4 h, HCT-116 cells in the PDT groups were subjected to 5 min of irradiation with a 670 nm laser (50 mW/cm^2) (PDT irradiation) and washed with PBS to remove the excess formulations. Finally, freshly prepared medium was added to the cells, which were incubated for 24 h at 37 °C. Subsequently, 5 mg/mL MTT solution was added to each well for 4 h, and the resulting formazan crystals were dissolved by adding 160 μL of DMSO. Finally, a microplate reader was used to measure the absorbance at 570 nm (BioTek, Winooski, Vermont, USA).

After incubation with DOX-Ce6 NPs or HA-DOX-Ce6 NPs, the cells were irradiated with PDT and incubated for 24 h. A Zeiss microscope (Zeiss Axio, Germany) was used to visualize the cellular morphology.

The cells were stained with Annexin V-FITC/propidium iodide (PI) to determine the degree of apoptosis resulting from the chemotherapy and PDT of the HA-DOX-Ce6 NPs. HCT-116 cells (5×10^5/well) were seeded into 6-well plates overnight, which were then treated with nanoparticles and irradiated as described previously. After incubation for 24 h, Annexin V-FITC/PI was added for 15 min, after which the cells were stained in the dark according to specific instructions and then collected before being analyzed by flow cytometry (BD Biosciences, CA, USA).

HA-DOX-Ce6 NP Distribution in vivo

We determined the distribution of HA-DOX-Ce6 NPs in tumor-bearing and tumor-bearing mice in vivo. For the tumor distribution study, after the tumor grew to 80 mm^3, DOX solution, Ce6 solution, DOX-Ce6 NPs, or HA-DOX-Ce6 NPs were given to each tumor-bearing mouse through intravenous injection via the tail vein (DOX at 5 mg/kg). After 24 h of administration, the animals were sacrificed, and the tumor tissues were dissected. Subsequently, the tumor tissues were frozen and sectioned, followed by 4% (w/w) formaldehyde fixation and DAPI staining. CLSM was used to detect the NP distribution.

Owing to the potent fluorescence emission within the deep red light region of Ce6, the biodistribution of HA-DOX-Ce6 NPs could be evaluated by fluorescence imaging analysis. Following 24 h of treatment with Ce6 solution, DOX-Ce6 NPs, or HA-DOX-Ce6 NPs, the animals were sacrificed, and their heart, spleen, lung, liver, kidney, and tumor tissues were collected and observed using an in vivo imaging system (Xenogen, Alameda, CA).

Antitumor Efficacy of HA-DOX-Ce6 NPs in vivo

For in vivo studies, we inoculated BALB/c nude mice with 2×10^6 HCT-116 cells via subcutaneous injection into the right forelimb armpit. After the tumors grew to 80 mm^3, we divided the tumor-bearing mice into six groups (n = 5): PBS, DOX solution, Ce6 solution (+PDT), DOX-Ce6 NPs (+PDT), HA-DOX-Ce6 NPs, and HA-DOX-Ce6 NPs (+PDT). Then, a 5 mg/kg dose of the DOX formulation was injected into the mice via the tail vein at 2-day intervals three times. For the PDT treatment, at 24 h postinjection, the mice were irradiated for 10 min at 670 nm (50 mW/cm^2), whereas those in the control group were injected with PBS.

The tumor volume and body weight of the mice were measured daily. The tumor volume was calculated as follows: (length × width^2)/2. On day 24, the animals were sacrificed, and major organs and tumors were dissected and fixed in a 4% (w/w) formaldehyde solution. Then, the isolated tumors were photographed and weighed. The tumor inhibitory rate (TIR) was calculated as follows: tumor weight in the control group - tumor weight in the tested group/tumor weight in the control group × 100%. These excised tumor tissues were subjected to H&E staining for pathological analysis.

To evaluate the systemic toxicity of each prepared formulation, the excised major organs, including the heart, spleen, liver, kidney, and lung, were subjected to H&E staining for histopathological analysis.[33] A colorimetric TUNEL assay was subsequently performed to observe and quantify cell apoptosis on tumor tissue slides, and the cell apoptosis rate was determined.

Statistical Analysis

Statistical analysis was performed via SPSS 18.0 software. Student's *t* test and one-way ANOVA followed by SNK or Dunnett's *t* test were performed for data analysis. A p value of <0.5 was considered to indicate statistical significance. The data are presented as the means ±SDs.

Results

Preparation and Characterization of HA-DOX-Ce6 NPs

Self-assembly is a drug delivery strategy that plays an important role in the nanotechnology and biomedicine fields.[34,35] In this study, we used an improved, easy, and environmentally friendly self-assembly method to fabricate NPs that synergize the efficacy of chemotherapy and PDT. The preparation scheme for the HA-DOX-Ce6 NPs is shown in Figure 2. Ce6 consists of a hydrophobic porphyrin ring and three carboxyl groups. The carboxyl groups gain negative charges in a strong alkaline solution (pH 12.0, NaOH). The pKa value of the primary amine group in DOX was reported to be 8.2–9.9,[36] thus it may have a positive charge at acidic and neutral pH values. Under neutral conditions, DOX and the photosensitizer Ce6 can spontaneously polymerize into NPs via electrostatic interactions under simple mixing conditions without the need for organic solvents. Additionally, the hydrophobic nature of Ce6 and the aromatic ring of DOX facilitate hydrophobic and π–π stacking interactions, further contributing to the formation of NPs.[30] Dynamic light scattering analysis revealed that the nanoparticles were small (198 ±2.1 nm) with a relatively narrow size distribution (Figure 3A).

To achieve tumor-targeted delivery, CD44 ligand-HA was modified into NPs via electrostatic interactions between the anionic-charged HA and the positively charged DOX. Following modification with HA, the zeta potential of the DOX-Ce6 NPs ranged from −16.80 ±0.31 mV to −18.30 ±0.19 mV (Figure 3E-F). This change in zeta potential indicates sufficient physical stability resulting from electrostatic repulsion. The negative charge helps improve NP stability, prevents nonspecific binding of NPs to plasma proteins in the blood, and increases the in vivo circulation time of NPs.[37] Furthermore, because of the spatial site resistance effect of HA, the particle size increased upon HA modification,

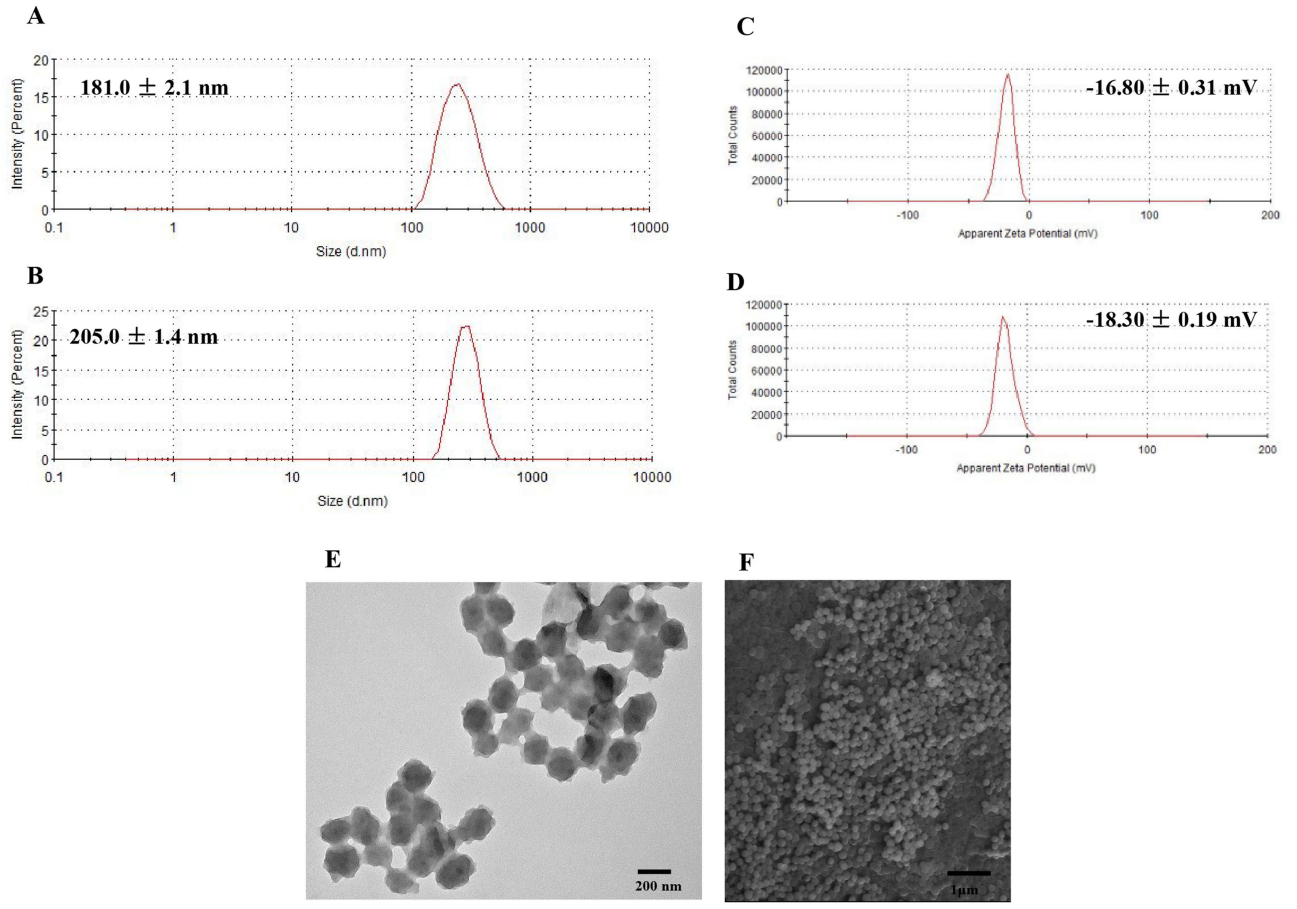

Figure 3 The size distributions of (**A**) DOX-Ce6 NPs and (**B**) HA-DOX-Ce6 NPs; Zeta potential of, (**C**) DOX-Ce6 NPs, and (**D**) HA-DOX-Ce6 NPs. TEM (**E**) and SEM (**F**) images for HA-DOX-Ce6 NPs.

https://doi.org/10.2147/IJN.S490485

resulting in an average HA-DOX-Ce6 NP size of 205.0 ±1.4 nm (Figure 3B). NPs of this size are advantageous as they help to evade clearance by the reticuloendothelial system (RES).[38] The particle size and zeta potential serve as indicators of successful HA modification. The morphology of the HA-DOX-Ce6 NPs was further characterized via TEM and SEM. TEM and SEM revealed that the NPs were in a dry state but exhibited regular spherical and uniformly distributed shapes (Figure 3C-D).

The effects of the DOX/Ce6 ratio and the DOX concentration on the size, PDI, drug-loading efficiency, and encapsulation efficiency of the HA-DOX-Ce6 NPs were evaluated. When the DOX/Ce6 ratio increased, the NP size increased significantly. However, the PDI was hardly affected (Figure 4A). However, both the LE and EE of HA-DOX-Ce6 for DOX or Ce6 were significantly affected by the DOX/Ce6 ratio. Specifically, the drug-loading efficiency of DOX increased gradually with increasing DOX/Ce6 ratio, whereas the opposite trend was observed for the drug-loading efficiency of Ce6. Similarly, the encapsulation efficiency showed the opposite trend compared with the drug-loading efficiency for DOX and Ce6 (Figure 4B). The effect of the DOX concentration was subsequently investigated. As the DOX concentration increased, the particle size increased, whereas the PDI was not significantly affected (Figure 4C). Notably, when the DOX concentration increased from 10 to 20 mg/mL, the particle size increased considerably from 80 nm to 370 nm, indicating enhanced aggregation. With increasing DOX feeding weight, the LE of DOX slightly increased, but the encapsulation rate decreased rapidly. Conversely, for Ce6, the drug-loading efficiency slightly decreased, whereas the encapsulation rate increased significantly with increasing DOX concentration (Figure 4D). Considering the requirement for sufficient Ce6 and DOX in the combination treatment, a DOX/Ce6 ratio of 1:1 and a DOX concentration of 15 mg/mL were determined to be the optimal formulations for subsequent experiments.

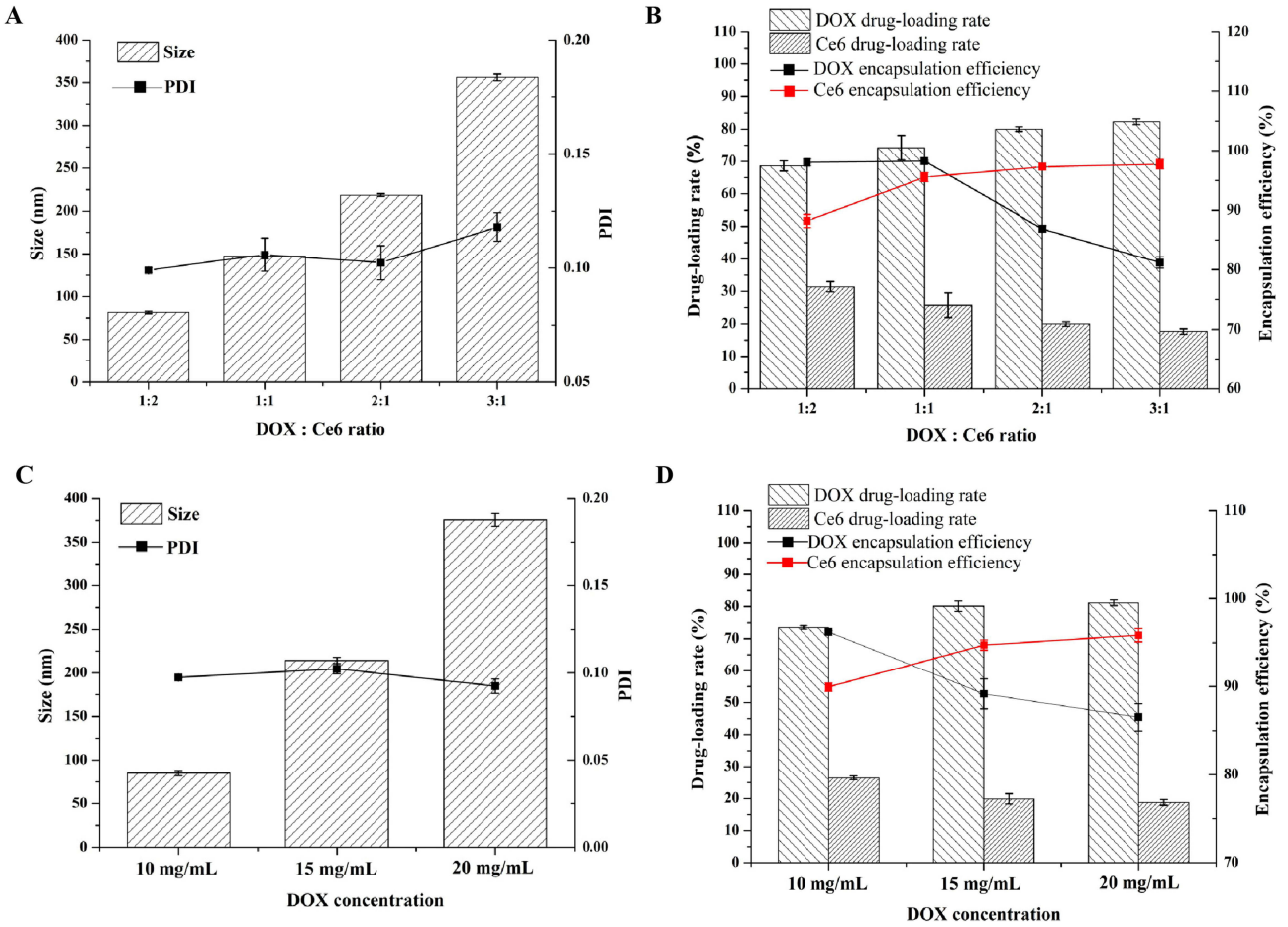

Figure 4 The effects of DOX/Ce6 ratio on the (**A**) size or PDI and (**B**) drug-loading rate or encapsulation rate of DOX and Ce6. Effect of DOX concentration on (**C**) size or PDI and (**D**) drug-loading rate or encapsulation rate. Results are presented as mean ±SD (n = 3).

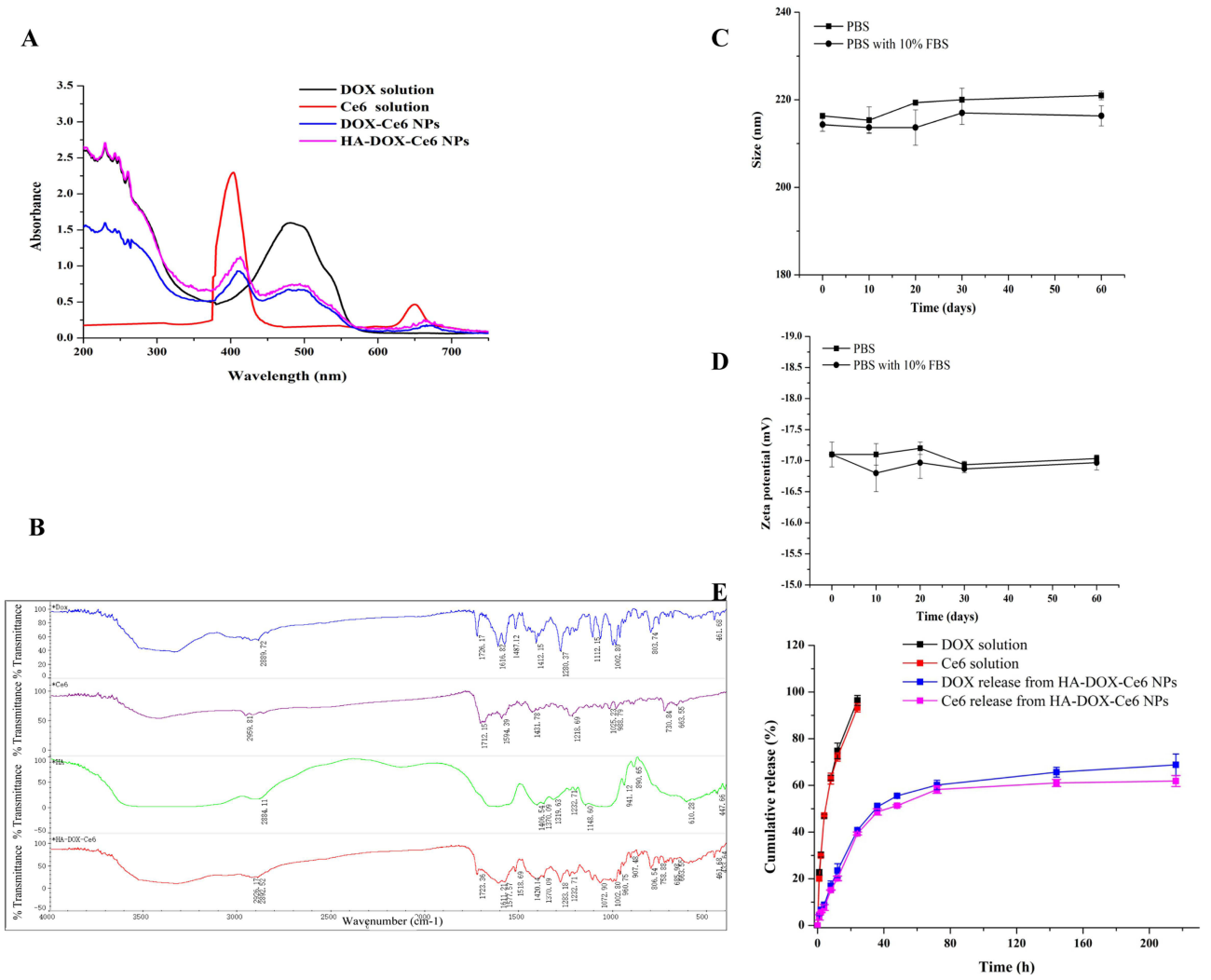

Figure 5 (**A**) UV-vis spectra for the DOX solution, Ce6 solution, DOX-Ce6 NPs and HA-DOX-Ce6 NPs. (**B**) FT-IR spectra for DOX, Ce6, HA, and HA-DOX-Ce6 NPs. The stability of HA-DOX-Ce6 NPs evaluated by size (**C**) and zeta potential (**D**) changes in PBS or diluted with PBS containing 10% FBS by 10-fold and stored at 4 °C for 60 days. (**E**) In vitro DOX or Ce6 release profile of HA-DOX-Ce6 NPs at 37 °C. DOX solution and Ce6 solution were treated as control groups. Results are presented as mean ±SD (n = 3).

The successful coassembly of the NPs was confirmed through UV-Vis spectral analysis. As shown in Figure 5A, the DOX-Ce6 NPs presented the characteristic absorbance peaks of DOX (~250 and 495 nm) and Ce6 (400 and 655 nm). This confirmed the presence of both components within the DOX-Ce6 NPs, which self-assembled to form NPs through interactions, resulting in the physicochemical properties of both components. The broader and redshifted Soret band observed in Ce6, along with the redshifted absorption band in DOX, indicates that the interaction between the pyrrole moiety of Ce6 and the aromatic ring in DOX is facilitated by hydrophobicity and π–π interactions.[39] Because HA lacks UV absorption,[40] UV-Vis spectral analysis of the HA-DOX-Ce6 NPs revealed minimal differences compared with those of the DOX-Ce6 NPs, suggesting that the physicochemical characteristics of the nanoparticles remained unchanged following HA modification.

We conducted further analysis via FT-IR spectroscopy to confirm the successful grafting of HA-DOX-Ce6 (Figure 5B). The stretching vibrations (2926 cm^{-1} and 1420 cm^{-1}) of O-H in HA-DOX-Ce6 were intensified following the coupling of DOX (2889 cm^{-1} and 1412 cm^{-1}), Ce6, and HA, possibly due to the increased number of hydroxyl groups within the HA chain, resulting in a redshift of this band. Similarly, the peak at 1594 cm^{-1} corresponds to the stretching vibration of -COOH in Ce6, where the carboxyl peak of HA-DOX-Ce6 shifted to 1611 cm^{-1} after HA modification, possibly indicating enhancement due to the presence of multiple carboxyl groups. Additionally, the peak

https://doi.org/10.2147/IJN.S490485

observed at 1487 cm^{-1} was associated with the stretching vibration of the C-C benzene ring, whereas the characteristic peak of HA-DOX-Ce6 also appeared at 1512 cm^{-1} and redshifted with increasing conjugation system.

The stability of the HA-DOX-Ce6 NPs was assessed under various conditions (PBS with/without 10% FBS) at 4 °C for 60 days. These electrostatic, hydrophobic, and π–π stacking interactions contribute to the formulation stability of self-assembled NPs.[18,41] As shown in Figure 5C-D, no significant difference in particle size or zeta potential was observed after 60 days of storage in PBS. Furthermore, these self-assembled nanoparticles maintained physical stability in PBS containing 10% FBS, indicating good serum stability. From the TEM and SEM results also shown that the nanoparticles maintain a relatively stable nanoparticle size and morphology both in PBS (Figure S1A-B) or PBS with 10% serum (Figure S2 A-B). Consequently, HA-DOX-Ce6 NPs can be stored for extended periods while maintaining stability in the bloodstream,[42] which is favorable for drug efficacy.

Drug Release Profile of the HA-DOX-Ce6 NPs

Figure 5E shows the release profile of the HA-DOX-Ce6 NPs in vitro. In the free DOX or free Ce6 groups, a burst release pattern was observed, with nearly all drugs being released within the initial 20 h. However, sustained release was evident after the drugs were loaded into the nanoparticles. The drugs encapsulated within the PLGA material were efficiently released at a high level, ensuring adequate drug concentrations for in vivo treatment. About 55% of the Ce6 or DOX was released from the HA-DOX-Ce6 NPs within the initial 48 h, followed by sustained release over another 100 h. The release behaviors of Ce6 and DOX were similar, facilitating synergistic anticancer effects of PDT and chemotherapy in vivo. Additionally, this sustained release pattern enables continued resistance against tumor cells.[43] The drug release profile of HA-DOX-Ce6 NPs suggests their potential use as an injectable formulation for anticancer drug delivery.

ROS Detection

ROS generation indicates the efficacy of PDT, which is primarily responsible for cell death.[44] To determine the PDT effect of HA-DOX-Ce6 NPs, a sensitive indicator ROS-DPBF was used to perform the ROS generation test. Upon reaction with ROS, the uptake summit of DPBF was attenuated.[45] As shown in Figure 6A, the DPBF absorbance of the HA-DOX-Ce6 NPs sharply decreased from 400–600 nm after 10 min of laser irradiation at 670 nm, which decreased with increasing irradiation time. Compared with the HA-DOX-Ce6 NPs, the DOX-Ce6 NPs and Ce6 solution exhibited similar DPBF absorbances (Figure 6B-C). To evaluate the ROS levels, the fluorescence intensities of the Ce6 solution, DOX-Ce6 NPs, and HA-DOX-Ce6 NPs at an equivalent concentration in deionized water were determined at 670 nm irradiation. As shown in Figure 6D, no significant difference in the ROS production rate or amount was found among the Ce6 solution, DOX-Ce6 NPs, and HA-DOX-Ce6 NPs, indicating that Ce6 exhibited unchanged photodynamic efficiency after NP formation.

Cellular Uptake of HA-DOX-Ce6 NPs

We further evaluated the selective intracellular uptake of different formulations in HCT-116 cells by CLSM. As shown in Figure 7A, DOX and Ce6 emitted red fluorescence and green fluorescence in the cell nucleus and cytoplasm, respectively. After treatment with the DOX solution, the cells exhibited weak red fluorescence in the nucleus. Furthermore, negligible green fluorescence was observed in the cytoplasm after incubation with the Ce6 solution. We observed fluorescence in the cytoplasm and nucleus of the NP (DOX-Ce6 NP and HA-DOX-Ce6 NP)-treated groups compared with the free DOX- or free Ce6-treated groups. Notably, the fluorescence intensity of DOX or Ce6 in the HA-DOX-Ce6 NP-treated group was considerably greater than that in the DOX-Ce6 NP-treated group. The 3D integration of whole-cell intracellular fluorescence clearly revealed significant enhancement of Ce6 and DOX in the HA-DOX-Ce6 NP group. The results of quantitative experiments revealed that the DOX and Ce6 cellular levels in the HA-DOX-Ce6 NP-treated group were markedly greater than those in the DOX-Ce6 NP-treated group (Figure 7B). These results indicate that, compared with nonmodified NPs, HA-modified NPs exhibit significantly improved intracellular uptake levels. This improvement can be attributed to HA-induced active cells targeting the CD44 receptor on CD44-overexpressing cells. HCT-116 cells overexpress the HA receptor CD44.[46] Excessive HA ligands compete with HA-DOX-Ce6 NPs for

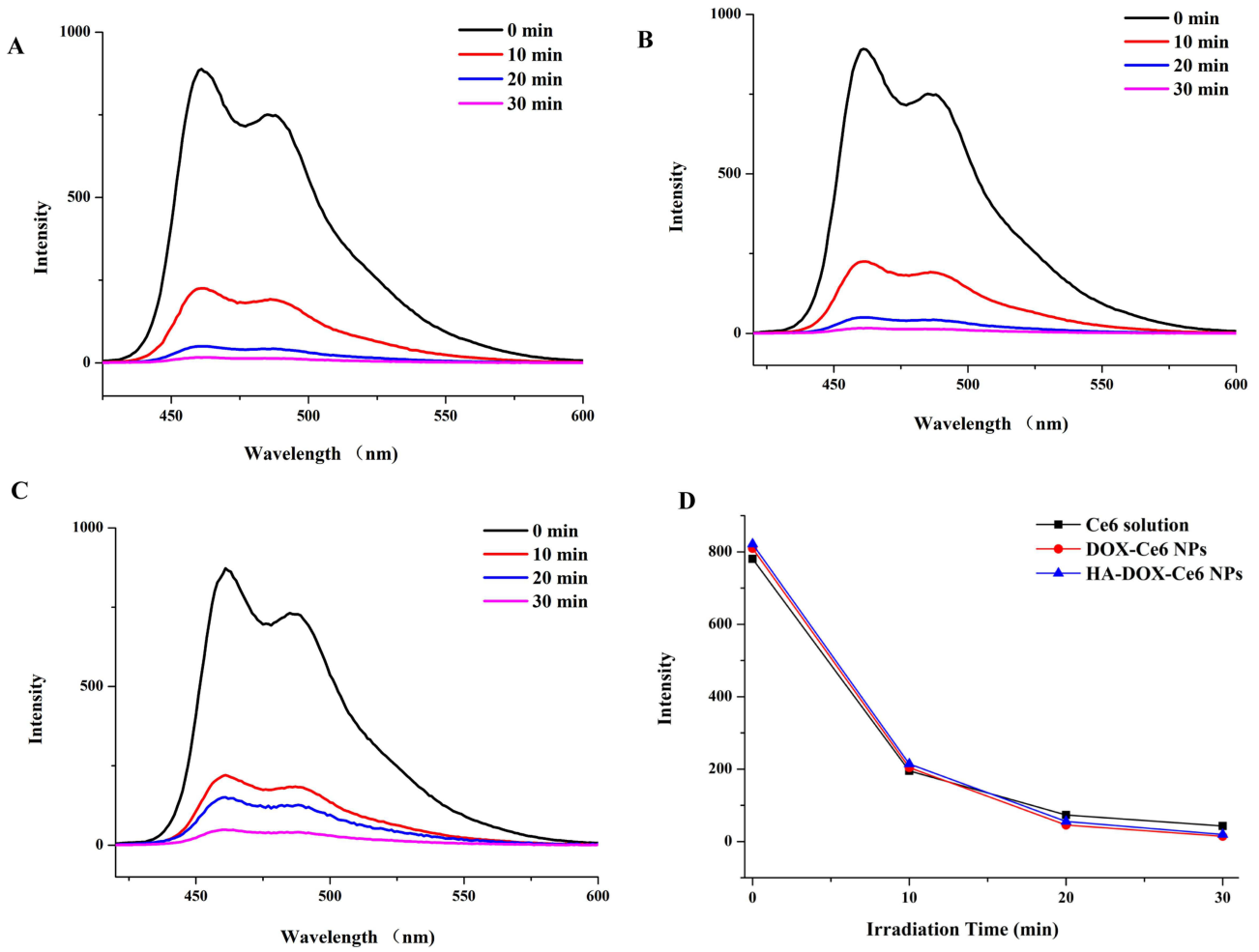

Figure 6 The absorbance spectra of DPBF after irradiation by 670 nm wavelength laser (50 mW/cm^2) with (**A**) HA-DOX-Ce6, (**B**) DOX-Ce6, and (**C**) Ce6 solution with different times. (**D**) Comparison between DPBF fluorescence intensity with Ce6 solution, DOX-Ce6, and HA-DOX-Ce6 at the same concentration (Ce6-equiv) after laser irradiation at 670 nm.

receptor binding, thereby considerably decreasing the endocytosis of HA-DOX-Ce6 NPs. Hence, the cytoplasmic and nuclear fluorescence intensities in the HA-DOX-Ce6 NP + HA-treated group decreased significantly. Based on the aforementioned results, HA-DOX-Ce6 NP uptake was CD44-mediated. Additionally, HA-decorated NPs promoted cellular absorption and improved tumor penetration through a CD44-mediated crosstalk cycle of endocytosis and exocytosis.[47]

Distribution of HA-DOX-Ce6 NPs in Cells

Additionally, the HA-DOX-Ce6 NP distribution within cells was examined via CLSM and TEM. As shown in Figure 7C, a higher concentration of HA-DOX-Ce6 NPs was observed in the lysosome-like vesicles. TEM images of the intracellular HA-DOX-Ce6 NPs revealed that the NPs maintained their structure after endocytosis. Additionally, after endocytosis, the NPs could achieve intracellular drug release and localization in targeted organelles. As shown in Figure 7D, lysosomes labeled with a lysosome tracker exhibited red fluorescence in the cytoplasm. After cellular endocytosis, the DOX released from the nanoparticles can enter the nucleus via the nuclear pore,[48] whereas the released Ce6 and NPs accumulate in the lysosomes. These findings imply that after being absorbed by cells, HA-DOX-Ce6 NPs can effectively release and distribute the drug to the target site, allowing the subsequent exertion of various pharmacological effects.

https://doi.org/10.2147/IJN.S490485

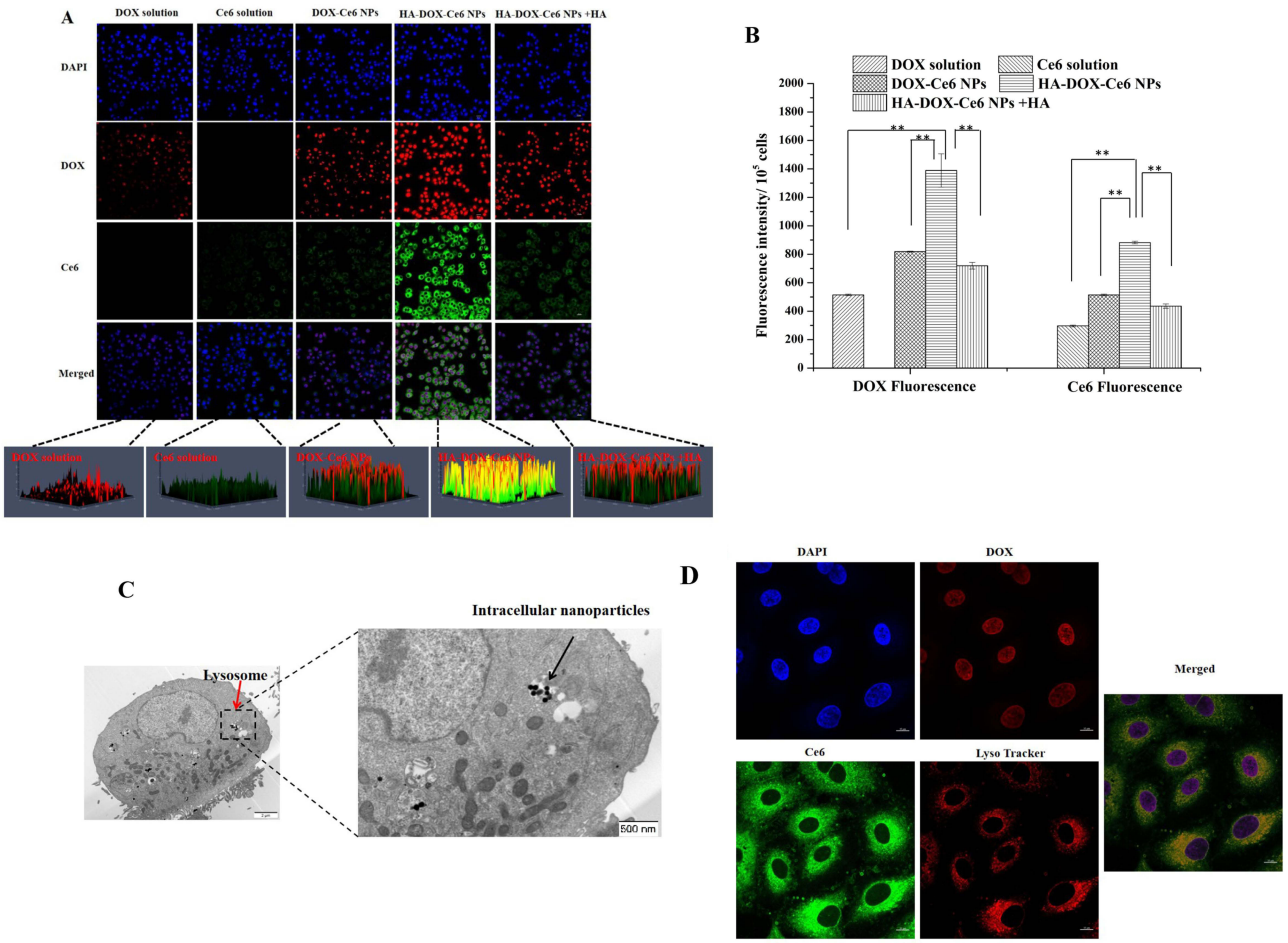

Figure 7 (**A**) CLSM images of HCT-116 cells after incubating with DOX solution, Ce6 solution, DOX-Ce6 NPs, HA-DOX-Ce6 NPs, and HA-DOX-Ce6 NPs combined with free HA. After nuclear staining with DAPI (blue), DOX shows red fluorescence, whereas Ce6 exhibits green fluorescence. Scale bar = 20 μm. (**B**) The DOX or Ce6 fluorescence intensity within HCT-116 cells (10^5) after DOX solution, Ce6 solution, DOX-Ce6 NPs, HA-DOX-Ce6 NPs and HA-DOX-Ce6 NPs combined with free HA treatment by a fluorescence spectrophotometry (**p < 0.01, versus HA-DOX-Ce6 NPs group). Intracellular distribution of HA-DOX-Ce6 NPs within HCT-116 cells. Cells were subjected to NP treatment and then observed by (**C**) TEM and (**D**) CLSM. The red arrows indicate lysosomes, and the black arrows indicate the intracellular nanoparticles in the TEM images. After DAPI nuclear staining (blue), DOX shows red fluorescence and colocalizes in the nucleus, Ce6 exhibits green fluorescence, and lysosomes exhibit red fluorescence and colocalize in the cytoplasm. Scale bar = 10 μm. Results are presented as mean ±SD (n = 3).

Detection of Cellular ROS During Irradiation

Based on our previous reports, HA-DOX-Ce6 NPs exhibited a noticeable yield of ROS production in DI water under laser irradiation at 670 nm. ROS generation is an important parameter of PDT. Higher ROS production by HA-DOX-Ce6 NPs indicates a greater improvement in the PDT effect on tumor cells. Hence, we used DCFH-DA as a ROS fluorescence indicator to evaluate ROS generation by HA-DOX-Ce6 NPs in HCT-116 cells. As shown in Figure 8, no green DCFH-DA fluorescence was detected within cells following treatment with the DOX solution, whereas obvious green fluorescence intensity was observed in the Ce6-treated groups, indicating that DOX cannot produce ROS. However, following treatment with HA-DOX-Ce6 NPs and 670 nm laser irradiation, potent green DCFH-DA fluorescence was observed, which was significantly greater than that in the free Ce6 or DOX-Ce6 NP groups. These findings indicate that ROS production considerably increased in the HA-DOX-Ce6 NP-treated group. This was possibly due to improved cellular absorption of HA-modified NPs, leading to sufficiently high intracellular production of ROS.

In summary, through intracellular absorption and ROS production analyses, we found that more drugs were internalized into CD44-overexpressing cells with the assistance of HA. Hence, HA-DOX-Ce6 NPs may exhibit improved anticancer activity compared with that of DOX-Ce6 NPs and DOX or Ce6 formulations.

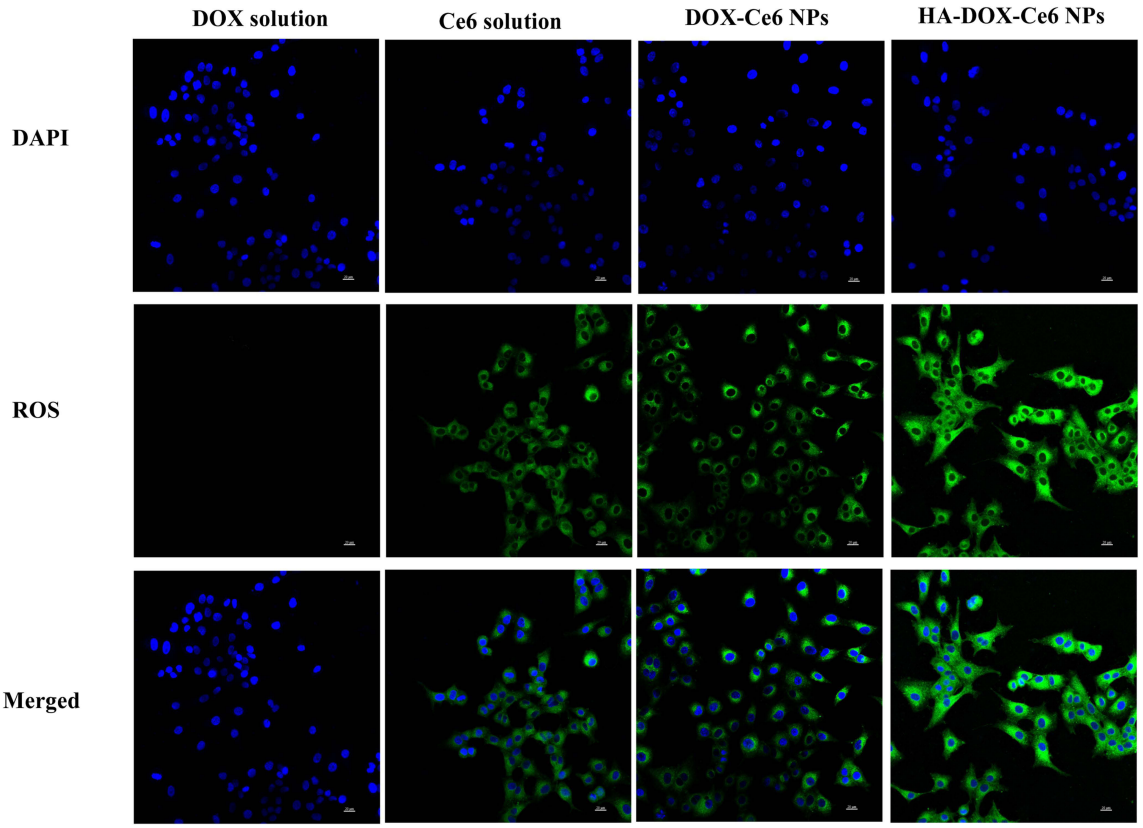

Figure 8 The intracellular ROS generation on HCT-116 cells. Cells were incubated with DOX solution, Ce6 solution, DOX-Ce6 NPs, and HA-DOX-Ce6 NPs after irradiation at 670 nm laser. After DAPI nuclear staining (blue), ROS shows green fluorescence. Scale bar = 20 μm.

Cytotoxicity of HA-DOX-Ce6 NPs in vitro

The MTT assay was performed to evaluate cell viability. As shown in Figure 9A, the DOX solution exhibited dose-dependent cytotoxicity in HCT-116 cells, with no significant difference in cell viability between the DOX solution and the DOX solution under PDT irradiation (Figure 9B). These results indicate that DOX cannot be activated under 670 nm irradiation and only exhibits a chemotherapeutic effect. However, no cytotoxicity was observed in cells treated with Ce6 solution without light irradiation. However, the Ce6 solution exerted a dose-dependent PDT effect upon 670 nm light irradiation, with cell viability decreasing to 43.2% at a Ce6 concentration of 10.56 μg/mL (equivalent to a DOX concentration of 22 μg/mL). Owing to their improved intracellular uptake, HA-DOX-Ce6 NPs demonstrated an efficient chemotherapeutic effect without laser irradiation, with cell viability decreasing to 37.1% at the 4.8 μg/mL Ce6 concentration (equivalent to a DOX concentration of 10 μg/mL). This decrease was significant compared with that in cells treated with DOX-Ce6 NPs (42.5%) or free DOX (56.5%) at the same concentration. Moreover, cell viability significantly decreased to 18.16% under 670 nm laser irradiation at a concentration of 4.8 μg/mL Ce6 in the HA-DOX-Ce6 NP group. The IC_{50} values were 5.6 ±0.32 and 3.2 ±0.26 μg/mL for HA-DOX-Ce6 and HA-DOX-Ce6 (+PDT), respectively (Figure 9C). These results indicate that HA modification improved the antitumor effect, with the HA-DOX-Ce6 NP group displaying the strongest anti-proliferative efficiency through a synergistic effect of chemotherapy and PDT.

The changes in cell morphology after treatment with all formulations are shown in Figure 9D. The morphology of HCT-116 cells became irregular and shrank after chemostimulation in the DOX-Ce6 NP- or HA-DOX-Ce6 NP-treated groups. Additionally, the number of cell debris, apoptotic bodies, chromatin granulation, and marginalization significantly increased in the HA-DOX-Ce6 NP (+PDT)-treated group.

Cell apoptosis due to the chemotherapy and PDT of the HA-DOX-Ce6 NPs was analyzed via Annexin-V-FITC/PI staining. As shown in Figure 9E and F, the Ce6 solution (+PDT) group exhibited a lower rate of apoptosis, which was

https://doi.org/10.2147/IJN.S490485

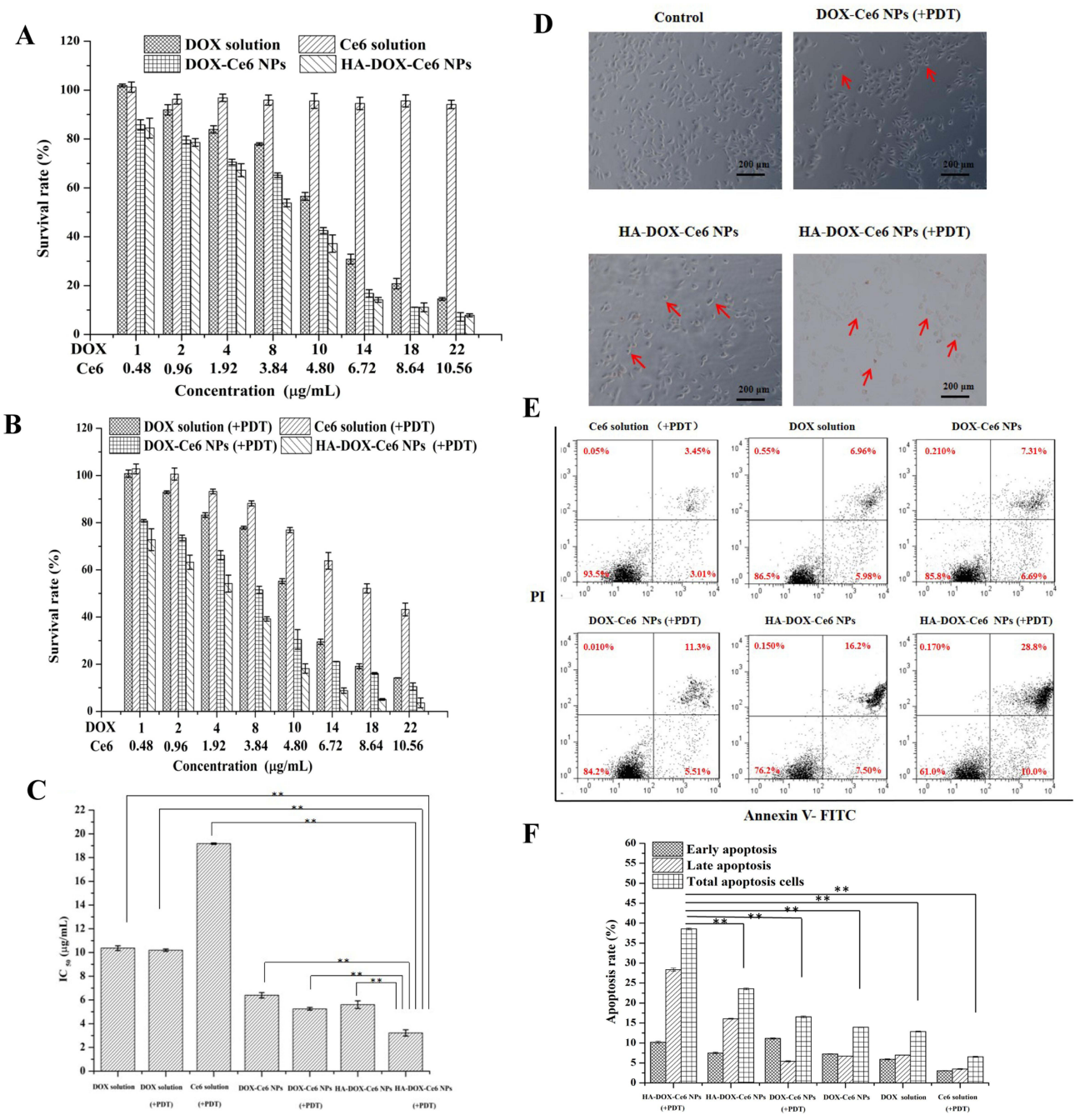

Figure 9 In vitro cytotoxicity of HA-DOX-Ce6 NPs was evaluated using HCT-116 cells by MTT assay. (**A**) Dark cytotoxicity and chemotherapy of DOX solution, Ce6 solution, DOX-Ce6 NPs, and HA-DOX-Ce6 NPs at the equivalent concentration. (**B**) Chemotherapy and PDT of DOX solution, Ce6 solution, DOX-Ce6 NP, and HA-DOX -Ce6 NP group after photostimulation by 670 nm laser. (**C**) IC_{50} values of DOX solution, DOX-Ce6 NPs, and HA-DOX-Ce6 NPs treated cells or under PDT (670 nm) treatment (**p < 0.01, vs HA-DOX-Ce6 NPs under PDT treatment group). (**D**) The morphology of the HCT-116 cells after DOX-Ce6 NP (+PDT) and HA-DOX-Ce6 NP treatment or PDT treatment with 3.0 μg/mL of DOX. The red arrows indicate apoptotic cells. (**E**) Cell apoptosis in HCT-116 cells after treatment using various formulations at the 3.0 μg/mL DOX concentration. (**F**) Quantification of cell apoptosis rate through flow cytometry with Annexin V-FITC/PI staining (**p < 0.01, versus HA-DOX-Ce6 NPs under PDT treatment group). Results are presented as mean ±SD (n = 3). Scale bar = 200 μm.

less than 10%. Compared with that in the DOX-Ce6 NP group, the percentage of apoptotic cells in the DOX solution group did not significantly differ, with values of 12.87 ±0.13% and 13.93 ±0.06%, respectively. Nevertheless, when the DOX-Ce6 NPs were exposed to PDT irradiation, the percentage of apoptotic cells increased to 16.56 ±0.24%. Similarly, the HA-DOX-Ce6 NP group showed a significantly increased apoptosis rate in HCT-116 cells (38.57 ±0.21%) after HA-DOX-Ce6 NP (+PDT) incubation compared with that in cells under chemotherapy alone, without PDT (23.57 ±0.23%).

These results suggest that the efficacy of the DOX-Ce6 NPs or HA-DOX-Ce6 NPs is enhanced by combining chemotherapy and PDT. In contrast to the HA-DOX-Ce6 NP (+PDT) group, after DOX-Ce6 (+PDT) treatment, HCT-116 cells exhibited considerably reduced apoptosis compared with that of cells under HA-DOX-Ce6 NP treatment and PDT irradiation. This finding indicates that the antitumor effect was improved after functionalization with HA. Furthermore, the constructed HA-DOX-Ce6 NPs exhibited sufficient antitumor effects when they reached the tumor tissue.

Distribution of HA-DOX-Ce6 NPs in vivo

Because Ce6 exhibits intrinsic near-infrared fluorescence in vivo, we can detect the distribution of HA-DOX-Ce6 NPs in tumor-bearing mice.[49] Tumor-bearing mice were injected with Ce6 solution, DOX-Ce6 NPs, or HA-DOX-Ce6 NPs in the tail vein. Then, the tumors and major organs were collected to observe their tumor-targeting ability and biodistribution. As shown in Figure 10A, only faint fluorescence or almost invisible fluorescence was observed in the liver, heart, spleen, kidneys, and lungs, suggesting that adverse effects on normal organs after intravenous injection can be ignored. Compared with those in the Ce6 solution group, the tumors collected from the DOX-Ce6 NP or HA-DOX-Ce6 NP group showed remarkable fluorescence. Furthermore, the HA-DOX-Ce6 NPs exhibited significantly improved fluorescence, suggesting increased tumor accumulation via the HA active-targeting and passive-targeting EPR effects. Additionally, the greater accumulation of HA-DOX-Ce6 NPs in tumor tissues verified the accumulation of DOX and Ce6, which improved the red fluorescence of DOX and the green fluorescence of Ce6 relative to those of free DOX, Ce6, and DOX-Ce6 NPs (Figure 10B).

Antitumor Effects of the HA-DOX-Ce6 NPs in vivo

Finally, we evaluated the effects of HA-DOX-Ce6 NPs on HCT-116 tumor-bearing mice. The treatment regimen is shown in Figure 10C. Tumor changes were monitored over 20 days. As shown in Figure 10D, the PBS, DOX solution, and Ce6 solution (+PDT) groups exhibited rapid tumor growth with no significant difference in tumor growth curves. A slight inhibition of tumor growth was observed in the DOX-Ce6 NP (+PDT)-treated group. However, the active-targeting capacity provided by HA modification promoted the anticancer effect of the HA-DOX-Ce6 NPs. Notably, HA-DOX-Ce6 NPs (+PDT) showed the maximum tumor inhibition among all the treatments (Figure 10E), indicating the superiority of combined PDT and chemotherapy with active-targeting capacity. After the experiment, the tumor weights were measured (Figure 10F-G). The tumors obtained from the HA-DOX-Ce6 NP (+PDT)-treated group were the smallest in size and weight, which is consistent with the results of the in vitro cytotoxicity and in vivo tissue distribution assays. The superior synergistic therapeutic effect of HA-DOX-Ce6 NPs (+PDT) was attributed to the advantages of nanosized drugs and combination therapies, including extended in vivo retention time, a passive-targeting effect of EPR, and an active-targeting effect of HA, leading to enhanced drug accumulation at the tumor site and simultaneous delivery of drugs with different mechanisms of action to the tumor mass, multipronged assault and so on. The tumor inhibition ratio was highest in the HA-DOX-Ce6 NP (+PDT) group, reaching 67.55 ±5.04% (Figure 10H), demonstrating the most potent antitumor effect. Compared with the PBS group, the DOX solution-treated group exhibited significant weight loss starting from the ninth day, with a total growth inhibition of 34.52 ±4.33%, whereas no marked difference was observed in the other groups, suggesting that post-nanoparticle treatment effectively reduced DOX toxicity (Figure 10G, I). Nevertheless, the occurrence of severe cardiotoxicity has prevented the widespread use of DOX in the clinic.[50,51] In this study, the toxicity of chemotherapy was mitigated via a carrier-free self-assembled nanoparticle approach. H&E staining of vital organs and tumor tissues was subsequently performed for histopathological examination. As shown in Figure 10J, the DOX-treated group exhibited slight myocyte degeneration, including myofiber necrosis and myocarditis in heart tissue, whereas no significant cardiac damage was observed in the organs of the other groups. However, the pathological characteristics of the tumors in the HA-DOX-Ce6 NP (+PDT) group differed from those in the PBS group. The initial growth of the tumor cells in the PBS, DOX, and Ce6 solution (+PDT) groups was maintained because of insufficient inhibition of tumor growth. Conversely, the tumor cells in the HA-DOX-Ce6 NP, with or without PDT, and DOX-Ce6 NP (+PDT) groups exhibited specific levels of apoptosis, with irregular shapes. Among the treatments, the HA-DOX-Ce6 NP (+PDT) group resulted in the most substantial tumor damage, indicating optimal antitumor efficacy.

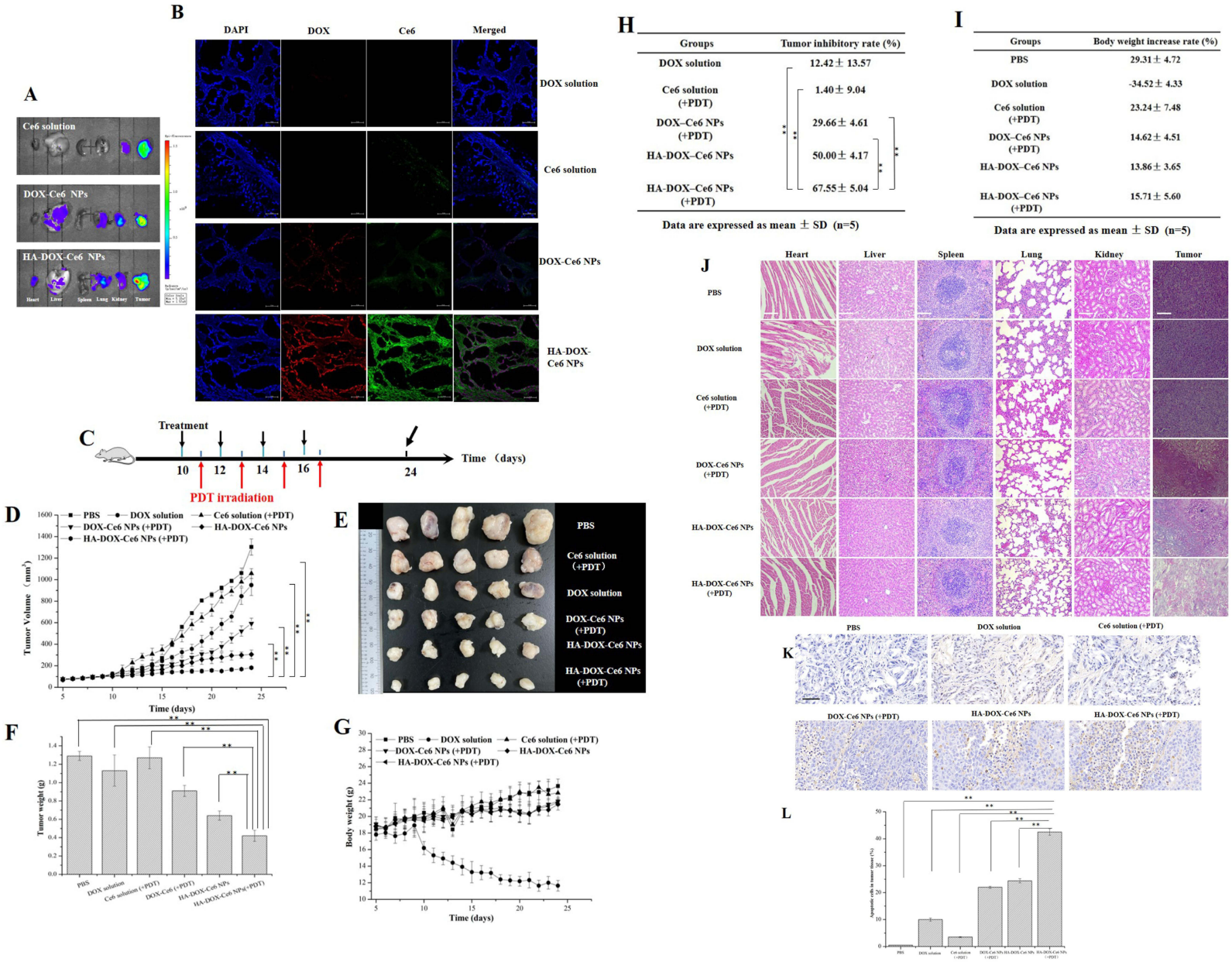

Figure 10 (**A**) Fluorescence images showing HA-DOX-Ce6 NP distribution in extracted tumors and organs after injection for 24 h. (**B**) CLSM images for tumor masses. After DAPI nuclear staining (blue), DOX exhibits red fluorescence, and Ce6 exhibits green fluorescence. Scale bar = 50 μm. Anticancer effect of HA-DOX-Ce6 NPs in vivo. (**C**) Experimental design for evaluation of the chemotherapy and PDT on tumor growth. Each formulation was injected into mice through the tail vein at the 5 mg/kg DOX concentration. Treatment parameters for PDT are 670 nm, 50 mW/cm^2, for 10 mins. (**D**) Tumor growth curves were assessed by recording the changes in tumor volume every day. (**E**) Representative photos of excised tumors of different groups. (**F**) Tumor weights of different groups after the experiment. (**p < 0.01, vs HA-DOX-Ce6 NPs in the PDT treatment group) (**G**) The changes of body weight in tumor-bearing mice following HCT-116 cell injection. (**H**) TIR of tumor-bearing mice was calculated after the experiment. (**I**) The body weight decrease rate of tumor-bearing mice was evaluated at the end of the experiment. (**J**) H&E staining data of the liver, heart, spleen, kidney, lung, and tumor in PBS, DOX solution, Ce6 solution (+PDT), DOX-Ce6 NP (+PDT), HA-DOX-Ce6 NP, and HA-DOX-Ce6 NP (+PDT) groups. Scale bar = 100 μm. (**K**) Apoptosis analysis by TUNEL assay. The brown color indicates the apoptotic cells. Scale bar = 100 μm. (**L**) Percentage of apoptotic cells in tumor tissues with various treatments. (**p < 0.01, vs HA-DOX-Ce6 NPs in the PDT treatment group).

TUNEL assay analysis of apoptosis in tumor tissues revealed significantly higher apoptosis rates in the NP-treated groups than in the DOX solution- or Ce6 solution (+PDT)-treated groups. Furthermore, the HA-DOX-Ce6 combined with PDT was the most effective apoptosis inducer, with the tumor cell apoptosis rate reaching 42.5 ±1.2%, which was significantly greater than that of the other groups (Figure 10K-L).

Discussion

Using nanotechnology to construct targeted nanodrug delivery systems can improve the solubility and delivery efficiency of traditional drugs, extend the half-life of drugs, increase their bioavailability, reduce adverse reactions, and solve the problem of drug resistance that arises in clinical treatment.[2,3] However, the efficacy, safety, pharmacokinetics and other drug-forming characteristics of novel nanodrug carriers still require in-depth and systematic studies. In addition, there are still some bottlenecks in the future of large-scale production of nanocarriers, such as low nanocarrier capacity, complex preparation of carrier materials, poor batch-to-batch controllability, high production costs, and potential systemic toxicity and immunogenicity, which largely limit their clinical application.[52,53] To achieve greater therapeutic efficacy, the concept of carrier-free nanodrugs has been proposed. This strategy is based on the self-assembly of drug molecules to form nanostructures with up to 100% drug loading capacity.[54] Compared with traditional nanodrug delivery systems, self-assembled carrier-free nanodrug delivery systems also have the following unique advantages: simple and flexible preparation methods, high drug loading capacity and delivery efficiency, long half-life in blood circulation, and avoidance of toxicity and immunogenic side effects associated with carriers. In recent years, carrier-free nanomedicines, such as antitumour, antimicrobial, anti-inflammatory and antioxidant nanomedicines, have been widely used in biomedical fields.[55] Self-assembly is a technique in which basic structural units (molecules, nanomaterials, micromaterials, etc.) spontaneously form an ordered structure. Currently, carrier-free nanomedicines are self-assembled mainly by weak noncovalent bonding forces such as hydrogen bonding, π-π stacking, hydrophobicity, electrostatic interactions, and van der Waals forces. In this study, HA-DOX-Ce6 nanoparticles were prepared via π-π stacking forces and electrostatic force-driven self-assembly of DOX with Ce6 and HA, resulting in a high drug loading capacity and uniform particle size, which is suitable for intravenous drug delivery.[36]

Tumors are currently the main cause of death worldwide, and chemotherapy remains one of the most important means of antitumor therapy.[1] DOX is a widely used anthracycline-based broad-spectrum antitumor drug in clinical practice, but its therapeutic efficacy is limited by its serious side effects, including cumulative cardiotoxicity and dose-limiting myelosuppression.[56] Researchers have long worked to find ways to reduce the toxic side effects of DOX. Combination therapy with two or more drugs has gradually become a new trend in the treatment of tumors. An appropriate combination of drugs can use different mechanisms to regulate the signaling pathway, restore the sensitivity of tumor cells to chemotherapeutic drugs, reverse the MDR of tumor cells, reduce the dosage of drugs while lowering the toxicity and side effects of the drugs, and exert a better antitumor effect than single-drug treatment does.[57] PDT, as a novel antitumour therapy, has become an effective treatment strategy for superficial and cavernous tumors because of its high target specificity, low invasiveness, low systemic toxicity and repeatability.[26] In recent years, the combination of chemotherapy and photodynamic therapy for malignant tumors has been gradually applied in clinical practice and has achieved improved therapeutic effects. On the one hand, photodynamic therapy can assist chemotherapy in enhancing target specificity and enhancing drug enrichment in the tumor area by changing vascular permeability; on the other hand, chemotherapy can assist photodynamic therapy in removing residual tumor cells and inhibiting the regeneration of damaged blood vessels.[58–60] The combination of these two therapies can enhance antitumor efficacy, reduce systemic toxic side effects, and may also overcome multidrug resistance (MDR) in tumor cells.[61] In this study, we found that, compared with the DOX solution group, both the DOX-Ce6 nanoparticles and HA-modified nanoparticles were able to show low toxicity to organs after intravenous injection, especially significantly reducing the toxicity to the heart, which was due to the protective effect of the nanoparticles, which was achieved by avoiding direct contact between the drug and the organ. On the other hand, passive/active targeting of the nanoparticles reduced the drug enrichment in the heart, ultimately demonstrating a favorable biosafety profile. The targeting effect of HA and the fact that PDT enhances the permeability of the tumor vasculature both increase the uptake of nanoparticles by tumor cells,[62] demonstrating enhanced antitumor effects. Chemo-photodynamic combination therapy is not a simple superposition of the two modalities. Under

the combined effect, biological processes such as tumor vascular effects and immune activation respond to the action of drugs and play important roles in combating the development of tumors. Based on the above advantages, chemo-photodynamic combination therapy is also used in clinical practice, especially for advanced patients who cannot tolerate surgery or who do not want to undergo surgery. Chemo-photodynamic combination therapy can strengthen the local tumor eradication effect, which can significantly improve the quality of survival and prolong the survival period of middle- and late-stage cancer patients.[63,64]

Conclusion

In this study, DOX, Ce6, and HA were successfully prepared via electrostatic interactions, π–π stacking, and hydrophobic interactions to obtain HA-DOX-Ce6 NPs without the use of a biocarrier material. HA-DOX-Ce6 NPs with a small size, regular spherical shape, and good stability exhibited efficient ROS production. HA-DOX-Ce6 NPs exhibited improved cytotoxicity against CD44-overexpressing HCT-116 cells and the most potent cytotoxicity after combining chemotherapy and PDT. Cellular uptake studies reported that HA-DOXCe6 NPs improved cellular uptake via CD44-mediated endocytosis, increasing the drug concentration in the target area. In vivo studies revealed improved tumor targeting, antitumor activity, and few side effects of HA-DOX-Ce6 NPs (+PDT) compared with those of the DOX solution, Ce6 solution (+PDT), and DOX-Ce6 NP (+PDT) formulations. In conclusion, HA-DOX-Ce6 NPs can synergize with the combined targeted therapeutic effects of chemotherapy and PDT.

Funding

This work is funded by the Natural Science Foundation of Zhejiang Province, China (LQ22H120004) and the Wenzhou Science and Technology Development Funds (Y2020832,Y20211017).

Disclosure

Our authors claim no competing interests.

References

1. Hu XY, Song Z, Yang ZW, Li JJ, Liu J, Wang HS. Cancer drug resistance related microRNAs: recent advances in detection methods. *Analyst*. 2022;147:2615–2632. doi:10.1039/D2AN00171C
2. Liu L, Eckert MA, Riazifar H, Kang DK, Agalliu D, Zhao W. From blood to the brain: can systemically transplanted mesenchymal stem cells cross the blood-brain barrier?. *Stem Cells Int*. 2013 2013;435093.
3. Wei T, Chen C, Liu J, Liu C, Peng L. Anticancer drug nanomicelles formed by self-assembling amphiphilic dendrimer to combat cancer drug resistance. *Proc Natl Acad Sci U S A*. 2015;112:2978–2983. doi:10.1073/pnas.1418494112
4. Zhang W, Shen J, Su H, et al.. Co-delivery of cisplatin prodrug and chlorin e6 by mesoporous silica nanoparticles for chemo-photodynamic combination therapy to combat drug resistance. *Acs Appl Mater Interfaces*. 2016;8:13332–13340. doi:10.1021/acsami.6b03881
5. Park K. Controlled drug delivery systems: past forward and future back. *J Control Release*. 2014;190:3–8. doi:10.1016/j.jconrel.2014.03.054
6. Bayda S, Adeel M, Tuccinardi T, Cordani M, Rizzolio F. The history of nanoscience and nanotechnology: from chemical-physical applications to nanomedicine. *Molecules*. 2019;25(1):112. doi:10.3390/molecules25010112
7. Yang X, Yang M, Bo P, Vara M, Xia Y. Gold nanomaterials at work.In: editor. *Nanomaterials and Neoplasms.*:2020.
8. Phung DC, Nguyen HT, Tran TTP, et al.. Combined hyperthermia and chemotherapy as a synergistic anticancer treatment. *J Pharm Investig*. 2019;49:519–526. doi:10.1007/s40005-019-00431-5
9. Lammers T, Kiessling F, Hennink WE, Storm G. Drug targeting to tumors: principles, pitfalls and (pre-) clinical progress. *J Control Release*. 2012;161:175–187. doi:10.1016/j.jconrel.2011.09.063
10. Parekh G, Shi Y, Zheng J, Zhang X, Leporatti S. Nano-carriers for targeted delivery and biomedical imaging enhancement. *Therap Delivery*. 2018;9:451–468. doi:10.4155/tde-2018-0013
11. Ruiz-Hernandez E, Lopez-Noriega A, Arcos D, Vallet-Regi M. Multifunctional nano and microparticles for drug delivery systems</u>. *Key Eng Mater*. 2010;441:333–355. doi:10.4028/www.scientific.net/KEM.441.333
12. Yu LD, Chen Y, Wu MY, et al.. "manganese extraction" strategy enables tumor-sensitive biodegradability and theranostics of nanoparticles. *J Am Chem Soc*. 2016;138:9881–9894. doi:10.1021/jacs.6b04299
13. Min YZ, Caster JM, Eblan MJ, Wang AZ. Clinical translation of nanomedicine. *Chem Rev*. 2015115:11147–11190. doi:10.1021/acs.chemrev.5b00116
14. Sosnik A. Reversal of multidrug resistance by the inhibition of ATP-binding cassette pumps employing "Generally Recognized As Safe" (GRAS) nanopharmaceuticals: a review. *Adv Drug Delivery Rev*. 2013;65:1828–1851. doi:10.1016/j.addr.2013.09.002
15. Huang P, Wang DL, Su Y, et al.. Combination of small molecule prodrug and nanodrug delivery: amphiphilic drug-drug conjugate for cancer therapy. *J Am Chem Soc*. 2014;136:11748–11756. doi:10.1021/ja505212y
16. Fu S, Li G, Zang W, Zhou X, Shi K, Zhai Y. Pure drug nano-assemblies: a facile carrier-free nanoplatform for efficient cancer therapy. *Acta Pharmaceutica Sinica*. 2022;12:92–106. doi:10.1016/j.apsb.2021.08.012

17. Shim MK, Yang S, Sun IC, Kim K. Tumor-activated carrier-free prodrug nanoparticles for targeted cancer Immunotherapy: preclinical evidence for safe and effective drug delivery. *Adv Drug Delivery Rev*. 2022183:22.
18. Yu F, Chen JX, Wei ZZ, et al.. Preparation of carrier-free astaxanthin nanoparticles with improved antioxidant capacity. *Frontiers Nutrition*. 2022;9:8.
19. Jiang SL, Fu Y, Zhang XY, Yu T, Lu BW, Du J. Research progress of carrier-free antitumor nanoparticles based on phytochemicals. *Front Bioeng Biotechnol*. 20219:8.
20. Ganipineni LP, Danhier F, Preat V. Drug delivery challenges and future of chemotherapeutic nanomedicine for glioblastoma treatment. *J Control Release*. 2018;281:42–57. doi:10.1016/j.jconrel.2018.05.008
21. Wei GQ, Wang Y, Yang G, Ju R, Ju R. Recent progress in nanomedicine for enhanced cancer chemotherapy. *Theranostics*. 2021;11:6370–6392. doi:10.7150/thno.57828
22. Cao W, Gu YW, Meineck M, Xu HP. The combination of chemotherapy and radiotherapy towards more efficient drug delivery. *Chemistry-an Asian J*. 2014;9:48–57. doi:10.1002/asia.201301294
23. Cao Y, Wang BC, Lou DS, Wang YZ, Hao SL, Zhang L. Nanoscale delivery systems for multiple drug combinations in cancer. *Future Oncol*. 2011;7:1347–1357. doi:10.2217/fon.11.109
24. Sauter ER. Cancer prevention and treatment using combination therapy with natural compounds. *Expert Rev Clin Pharmacol*. 2020;13:265–285. doi:10.1080/17512433.2020.1738218
25. Kimura M, Miyajima K, Kojika M, Kono T, Kato H. Photodynamic therapy (PDT) with chemotherapy for advanced lung cancer with airway stenosis. *Int J Mol Sci*. 2015;16:25466–25475. doi:10.3390/ijms161025466
26. Yu Y, Wang N, Wang YY, et al.. Photodynamic therapy combined with systemic chemotherapy for unresectable extrahepatic cholangiocarcinoma: a systematic review and meta-analysis. *Photodiagn Photodyn Ther*. 202341:8.
27. Menilli L, Milani C, Reddi E, Moret F, Panthong W, Ekalaksananan T. Overview of nanoparticle-based approaches for the combination of photodynamic therapy (PDT) and chemotherapy at the preclinical stage. *Cancers*. 2021;14:31. doi:10.3390/cancers14010031
28. Kwiatkowski S, Knap B, Przystupski D, et al.. Photodynamic therapy - mechanisms, photosensitizers and combinations</u>. *Biomed Pharmacother*. 2018;106:1098–1107. doi:10.1016/j.biopha.2018.07.049
29. Spring BQ, Rizvi I, Xu N, Hasan T. The role of photodynamic therapy in overcoming cancer drug resistance. *Photochem Photobiol Sci*. 2015;14:1476–1491. doi:10.1039/c4pp00495g
30. Zhang RY, Xing RR, Jiao TF, et al.. Chemophotodynamic dual nanodrugs via self-assembly for synergistic antitumor therapy. *ACS Appl Mater Interfaces*. 2016;8:13262–13269. doi:10.1021/acsami.6b02416
31. Seo JY, Lee SY, Hwang CR, et al.. Multi-layered cellulose nanocrystal system for CD44 receptor-positive tumor-targeted anticancer drug delivery. *Int J Biol Macromol*. 2020;162:798–809. doi:10.1016/j.ijbiomac.2020.06.193
32. Wang XL, Ouyang XM, Chen JL, Hu Y, Sun XY, Yu ZW. Nanoparticulate photosensitizer decorated with hyaluronic acid for photodynamic/photothermal cancer targeting therapy. *Nanomedicine*. 2019;14:151–167. doi:10.2217/nnm-2018-0204
33. Koo JS, Lee SY, Nam S, et al.. Preparation of cupric sulfate-based self-emulsifiable nanocomposites and their application to the photothermal therapy of colon adenocarcinoma. *Biochem Biophys Res Commun*. 2018;503:2471–2477. doi:10.1016/j.bbrc.2018.07.002
34. Weiss PS, Kotov NA. Self-assembly of nanoparticles: a snapshot. *Acs Nano*. 2014;8:3101–3103. doi:10.1021/nn502057r
35. Grzelczak M, Vermant J, Furst EM, Liz-Marzan LM. Directed self-assembly of nanoparticles. *Acs Nano*. 2010;4:3591–3605. doi:10.1021/nn100869j
36. Alves AC, Magarkar A, Horta M, et al.. Influence of doxorubicin on model cell membrane properties: insights from in vitro and in silico studies. *Sci Rep*. 2017;7:6343–6357. doi:10.1038/s41598-017-06445-z
37. Huang JB, Zhang H, Yu Y, et al.. Biodegradable self-assembled nanoparticles of poly (D,L-lactide-co-glycolide)/hyaluronic acid block copolymers for target delivery of docetaxel to breast cancer. *Biomaterials*. 2014;35:550–566. doi:10.1016/j.biomaterials.2013.09.089
38. Gaucher G, Dufresne MH, Sant VP, Kang N, Maysinger D, Leroux JC. (2005) block copolymer micelles: preparation, characterization and application in drug delivery. *J Control Release*. 2005;109:169–188. doi:10.1016/j.jconrel.2005.09.034
39. Liu K, Xing R, Zou Q, et al.. Simple peptide-tuned self-assembly of photosensitizers towards anticancer photodynamic therapy. *Angewandte Chemie Angewandte Chemie*. 2016;55:3036–3039.
40. Shariati A, Ebrahimi T, Babadinia P, Shariati FS, Cohan RA, Rabbani H. Synthesis and characterization of Gd</SUP><SUP>3+-loaded hyaluronic acid-polydopamine nanoparticles as a dual contrast agent for CT and MRI scans</u>. *Sci Rep*. 2023;13:12. doi:10.1038/s41598-022-27243-2
41. Wei X, Gong C, Shi S. (2009) Self-assembled honokiol-loaded micelles based on poly(-caprolactone)-poly(ethylene glycol)-poly(-caprolactone) copolymer</u>. *Int J Pharm*. 2009;369:170–175. doi:10.1016/j.ijpharm.2008.10.027
42. Ju-Hwan P, Hyun-Jong C, Dae-Duk K. Poly((D,L)lactic-glycolic)acid-star glucose nanoparticles for glucose transporter and hypoglycemia-mediated tumor targeting</u>. *Int j Nanomed*. 2017;12:7453–7467. doi:10.2147/IJN.S147668
43. Baek JS, Cho CW. Controlled release and reversal of multidrug resistance by co-encapsulation of paclitaxel and verapamil in solid lipid nanoparticles. *Int J Pharm*. 2015;478:617–624. doi:10.1016/j.ijpharm.2014.12.018
44. Rajendran M. Quinones as photosensitizer for photodynamic therapy: ROS generation, mechanism and detection methods. *Photodiagnosis Photodynamic Therapy*. 2016;13:175–187. doi:10.1016/j.pdpdt.2015.07.177
45. Mvango S, Mashazi P. Synthesis, characterization of copper oxide-gold nanoalloys and their peroxidase-like activity towards colorimetric detection of hydrogen peroxide and glucose. *Materials Sci Eng*. 2019;96:814–823. doi:10.1016/j.msec.2018.12.010
46. Mvango S, Mashazi P. Characteristics of CD44 alternative splice pattern in the course of human colorectal adenocarcinoma progression. *Mol Cancer*. 201211.
47. El-Dakdouki MH, Ellen P, Huang X. Development of drug loaded nanoparticles for tumor targeting. part 2: enhancement of tumor penetration through receptor mediated transcytosis in 3D tumor models. *Nanoscale*. 2013;5:3904–3911. doi:10.1039/c3nr90022c
48. Lin JT, Chen H, Wang D, Xiong L, Chen GB. Nuclear-targeted p53 and DOX co-delivery of chitosan derivatives for cancer therapy in vitro and in vivo. *Colloids Surf*. 2019;183:110440. doi:10.1016/j.colsurfb.2019.110440
49. Wu J, Hu X, Liu R, Zhang J, Song A, Luan Y. pH-responsive and self-targeting assembly from hyaluronic acid-based conjugate toward all-in-one chemo-photodynamic therapy. *J Colloid Interface Sci*. 2019;547:30–39. doi:10.1016/j.jcis.2019.03.087
50. Al-Shabanah OA, El-Kashef HA, Badary OA, Al-Bekairi AM, Elmazar MMA. Effect of streptozotocin-induced hyperglycaemia on intravenous pharmacokinetics and acute cardiotoxicity of doxorubicin in rats. *Pharmacological Res*. 200041:31–37.

51. Duhem N, Danhier F, Pourcelle V. Self-assembling doxorubicin–tocopherol succinate prodrug as a new drug delivery system: synthesis, characterization, and in vitro and in vivo anticancer activity. *Bioconjugate Chemistry*. 2014;25:72–81. doi:10.1021/bc400326y
52. Zhang X, Li N, Zhang S, et al.. Emerging carrier-free nanosystems based on molecular self-assembly of pure drugs for cancer therapy. *Med Res Rev*. 2020;40:1754–1775. doi:10.1002/med.21669
53. Cheng H, Hu H, Li G, et al.. Calcium titanate micro-sheets scaffold for improved cell viability and osteogenesis - ScienceDirect. *Chem Eng J*. 2020;389(1):124400.
54. Mei H, Cai SS, Huang DN, et al. Carrier-free nanodrugs with efficient drug delivery and release for cancer therapy: from intrinsic physicochemical properties to external modification. *BioactMater*. 2022;8:220–240.
55. Huang L, Zhao SJ, Fang F, et al. Advances and perspectives in carrier-free nanodrugs for cancer chemo-monotherapy and combination therapy. *Biomaterials*. 2021;268:120557. doi:10.1016/j.biomaterials.2020.120557
56. Cagel M, Grotz E, Bernabeu E, Moretton MA, Chiappetta DA. Doxorubicin: nanotechnological overviews from bench to bedside. *Drug Discovery Today*. 2017;22(2):270–281. doi:10.1016/j.drudis.2016.11.005
57. Jin H, Wang L, Bernards R. Rational combinations of targeted cancer therapies: background, advances and challenges. *Nat Rev Drug Discov*. 202312(22):213–234.
58. Chang JE, Yoon IS, Sun PL, Yi E, Jheon S, Shim CK. Anticancer efficacy of photodynamic therapy with hematoporphyrin- modified, doxorubicin-loaded nanoparticles in liver cancer. *J Photochem Photobiol*. 2014;140:49. doi:10.1016/j.jphotobiol.2014.07.005
59. Hasan T, Rizvi I, Bryan Q. The role of photodynamic therapy in over coming cancer drug resistance. *Photochem Photobiol Sci off J Eur Photochem Assoc Eur Soc Photobiol*. 2015;14(8):1476.
60. Cheng L, Wang C, Feng L, Yang K, Liu Z. Functional nanomaterials for phototherapies of cancer. *Chin J Clin Oncology*. 2014114:10869–10939.
61. Snyder JW, Greco WR, Bellnier DA, Vaughan L, Henderson BW. Photody namic therapy : a means to enhanced drug delivery to tumors. *Cancer Res*. 2003;63(23):8126–8131.
62. Araki T, Ogawara KI, Suzuki H, et al.. Augmented EPR effect by photo-triggered tumor vascular treatment improved therapeutic efficacy of liposomal paclitax el in mice bearing tumors with low permeable vasculature. *J Control Release*. 2015;200:106–114. doi:10.1016/j.jconrel.2014.12.038
63. Luo D, Li N, Carter KA, et al.. Rapid light triggered drug release in liposomes containing small amounts of unsaturated and porphyrin-phospholipids. *Small*. 2016;12(22):3039–3047. doi:10.1002/smll.201503966
64. Brown SB, Brown EA, Walker I. The present and future role of photodynamic therapy in cancer treatment. *Lancet Oncol*. 2004;5(8):497–508. doi:10.1016/S1470-2045(04)01529-3